HHS Public Access

Author manuscript

Cell. Author manuscript; available in PMC 2024 October 26.

Published in final edited form as:

Cell. 2023 February 02; 186(3): 607–620.e17. doi:10.1016/j.cell.2022.12.037.

Immunity to the microbiota promotes sensory neuron regeneration

Michel Enamorado[1], **Warakorn Kulalert**[1], **Seong-Ji Han**[1], **Indira Rao**[1,2], **Jeremie Delaleu**[1], **Verena M. Link**[1], **Daniel Yong**[1], **Margery Smelkinson**[6], **Louis Gil**[1], **Saeko Nakajima**[1,3], **Jonathan L. Linehan**[1,4], **Nicolas Bouladoux**[1], **Josette Wlaschin**[5], **Juraj Kabat**[6], **Olena Kamenyeva**[6], **Liwen Deng**[7], **Inta Gribonika**[1], **Alexander T. Chesler**[8], **Isaac M. Chiu**[7], **Claire E. Le Pichon**[5], **Yasmine Belkaid**[1,9,10,*]

[1]Metaorganism Immunity Section, Laboratory of Host Immunity and Microbiome, National Institute of Allergy and Infectious Diseases, National Institutes of Health, Bethesda, MD 20892, USA.

[2]Immunology Graduate Group, University of Pennsylvania, Philadelphia, PA 19104 USA.

[3]Present address: Department of Dermatology, Kyoto University Graduate School of Medicine, Sakyo, 606-8507 Kyoto, Japan.

[4]Present address: Department of Cancer Immunology, Genentech, South San Francisco, CA 94080, USA.

[5]*Eunice Kennedy Shriver* National Institute of Child Health and Human Development, National Institutes of Health, Bethesda, MD 20892, USA.

[6]Biological Imaging, Research Technology Branch, National Institute of Allergy and Infectious Diseases, National Institutes of Health, Bethesda, MD 20892, USA

[7]Department of Immunology, Harvard Medical School, Boston, MA 02115, USA.

[8]National Center for Complementary and Integrative Health, National Institutes of Health, Bethesda, MD 20892, USA.

[9]NIAID Microbiome Program, National Institute of Allergy and Infectious Diseases, National Institutes of Health, Bethesda, MD 20892, USA.

[10]Lead contact

Summary

[*]Corresponding author: ybelkaid@niaid.nih.gov.

Author contributions

ME and YB designed the study, experiments and wrote the original manuscript. ME performed the experiments, analyzed the data, and created the figures. S-JH assisted with neuronal regeneration experiments in the skin. SN and JLL contributed to create the SA1^{Tg} mice. OK and WK assisted with 2-photon experiment analysis. VML and LG analyzed RNA-seq data. JW and LD assisted with DRG neurons experiments. MS, JD, DY and KJ assisted with confocal image analysis. IR and IG assisted with *S. aureus* colonization experiments. NB assisted with flow experiments and figure design. IMC, ATC and CELP provided intellectual expertise and shared key methodologies. All the authors reviewed and contributed to edit the manuscript before submission. Correspondence and requests for materials should be addressed to Y.B: ybelkaid@niaid.nih.gov

Declaration of interests

The authors declare no competing interests.

Tissue immunity and responses to injury depend on the coordinated action and communication among physiological systems. Here, we show that, upon injury, adaptive responses to the microbiota directly promote sensory neuron regeneration. At homeostasis, tissue-resident commensal-specific T cells colocalize with sensory nerve fibers within the dermis, express a transcriptional program associated with neuronal interaction and repair, and promote axon growth and local nerve regeneration following injury. Mechanistically, our data reveal that the cytokine interleukin-17A (IL-17A) released by commensal-specific Th17 cells upon injury directly signals to sensory neurons via IL-17 receptor A, the transcription of which is specifically upregulated in injured neurons. Collectively, our work reveals that in the context of tissue damage, preemptive immunity to the microbiota can rapidly bridge biological systems by directly promoting neuronal repair and identifies IL-17A as a major determinant of this fundamental process.

Introduction

Restoration of tissue integrity and function following injury or infection is of fundamental importance for host survival. Barrier tissues are not only primary targets of the environment but also the ecological niche of resident microbes, referred to as the microbiota. As such, protection of barrier integrity is of mutual interest to the host and its microbiota[1].

The microbiota plays a fundamental role in the induction, education, and function of the mammalian immune system[1]. In turn, the immune system operates to sustain and restore tissue function in the context of microbial or environmental exposures. Host-microbiota dialogue is of particular importance at barrier sites that are both home to the microbiota and primary targets of environmental stressors. One of the mechanisms associated with such control occurs via the induction of long-lasting, microbiota-reactive T cells that can broadly promote tissue function including antimicrobial defense and epithelial regeneration[2–4]

All barrier tissues, including the skin, are also home to a dense network of sensory nerve fibers that are involved in the perception of touch, temperature, pain and itch[5–9]. Recent work reveals that in addition to these fundamental functions, sensory neurons can also influence other biological processes including host metabolism, inflammation, and protective immunity[5,10–13]. These emerging observations underscore our growing understanding of the profound interconnection among biological systems and more particularly between the immune and nervous systems.

In the context of infection or injury, host survival requires protection and restoration of all tissue components, each requiring specific repair programs. Repair of the peripheral nervous system and reinnervation of tissues is of particular importance to restore sensory recovery, as well as coordination of tissue reepithelialization, neovascularization and wound healing[14–16]. As such, identification of key mechanisms involved in the restoration of peripheral nerves represents an active area of research of high importance to reduce disability and enhance quality of life[17]. In response to microbial colonization, barrier sites constitutively harbor tissue-resident commensal-specific T cells. This implies that injury or infection occur in the context of recall responses to the microbiota. In this context, whether adaptive immunity and more particularly adaptive immunity to the microbiota contributes to peripheral nerve regeneration remains unknown. Based on the profound alliance between the microbiota and

its host, we hypothesized that the microbiota could also play an important role in bridging biological systems as a means to reinforce tissue protection.

Here, exploration of host-microbiota interactions allowed us to uncover a mechanism of peripheral neuronal repair orchestrated by commensal-specific T cells. More specifically, our work reveals that tissue-resident microbiota-specific T cells can directly promote neuronal repair upon injury and identifies IL-17A as a major determinant of this fundamental process.

Results

Staphylococcus aureus colonization-induced Th17 cells have no impact on host protection

Staphylococcus aureus (*S. aureus*) can exist as commensals for decades before behaving as a pathogen[18,19]. In this context, preemptive immunity acquired during commensalism may be of particular importance to protect and/or restore tissue integrity upon subsequent damage and/or infection.

To explore this possibility, we utilized a strain of *S. aureus* previously isolated from healthy murine skin (42F02)[20]. Following topical association (TA), *S. aureus* 42F02 colonized the skin for weeks with no changes in epidermal thickness and with minor neutrophil infiltrate (Figures S1A and S1B). This homeostatic relationship was associated with a strong accumulation of T cells within the skin compartment that was dominated by RORγt-expressing $CD4^+$ T (Th17) cells (Figures 1A and 1B). These responses peaked at 2 weeks post-association and lasted for at least 2 months (Figure 1A). In contrast, response to the same microbe as a pathogen (following intradermal injection, ID) was characterized by tissue damage, inflammation and highly polarized Th1 responses (Figures 1B, S1B and S1C). Consistent with T cell responses to other skin commensals[21,22], Th17 cell accumulation in the skin was dependent on the cytokine IL-1, live microbes, and intact lymphoid structures (Figures S1D–S1F).

To assess the specificity of Th17 responses to *S. aureus* colonization, we generated a TCR transgenic mouse ($SA1^{Tg}$), in which all T cells generated are reactive to *S. aureus*. Further highlighting the high diversity of *S. aureus*[23], expansion of transgenic T cells following association was only observed in response to 42F02 and not to other *S. aureus* strains tested (Figure S1G). $SA1^{Tg}$ cells were transferred to mice prior to topical association with *S. aureus,* and in line with polyclonal responses, *S. aureus*-specific T cells accumulated within the skin and dominantly developed as Th17 cells (Figures 1C and 1D). This was in contrast to infection with the same bacteria in which $SA1^{Tg}$ developed mostly as Th1 cells (Figure 1D).

Previous reports have proposed a protective role for IL-17 against *S. aureus* infection[24,25]. To assess whether Th17 responses to *S. aureus* as a commensal could provide protective immunity to subsequent infection, unassociated mice and mice previously colonized with *S. aureus* were infected intradermally with *S. aureus* (TA alone and TA+ID, respectively). Infection of mice previously colonized (TA+ID) promoted highly polarized Th17 recall responses (both polyclonal and antigen-specific) that lasted for at least seven days post-

intradermal infection (Figures 1E and 1F). These Th17 recall responses post-intradermal infection were dominant in mice previously associated with *S. aureus* as a commensal and not in mice previously infected with the same bacteria (Figure S1H). In contrast, previous infection dominantly recalled Th1 cells (Figure S1H). Despite potent Th17 recall responses, previous topical association had no impact on bacterial burden within the skin (Figure 1G). Furthermore, under these settings, protection was only observed within the regional lymph nodes (Figure 1H) and surprisingly the systemic bacterial control was IL-17A-independent, as demonstrated with *Il17a*$^{-/-}$ mice, mice treated with an anti-IL-17A blocking antibody and in mice deficient in Th17 cells (*Ox40*$^{Cre+}$*Rorc*$^{f/f}$) (Figures 1H, S1I and S1J). Thus, Th17 responses to *S. aureus* as a commensal have no impact on the ability of the host to develop local or systemic protection against subsequent *S. aureus* infection. These observations pointed to alternative roles for commensal-induced Th17 cells in tissue physiology.

Staphylococcus aureus-induced T cells express a neuronal regeneration transcriptomic signature

To explore the roles of *S. aureus*-induced Th17 cells in host physiology, we focused our analysis on the dominant immune responses associated with each treatment, namely Th17 induced by topical association (TA) and Th1 induced by intradermal infection (ID) (Figures 1A and 1B). To this end, we isolated Th17 (CCR6^{+}CD4^{+}Foxp3^{-}) and Th1-enriched cells (CCR6^{-}CD4^{+}Foxp3^{-}) from the skin of mice two weeks post-topical association (TA) and one week post-infection (ID) respectively for RNA-seq analysis (Figure 2A). As a control, antigen-experienced CD4^{+} T cells (TEM: CD44^{high}CD62L^{low}CD4^{+}Foxp3^{-}) were also isolated from the regional (auricular) lymph nodes of unassociated mice. Th17 cells from TA showed over 3000 differentially expressed transcripts compared to Th1 from ID (Figure S2A). As expected, genes associated with type 17 *(Il17a*, *Il17f*, *Il22, Ccr6*, *Rorc*, *Rora)* were more highly expressed in Th17 (TA) (Figure 2A). Consistent with the role of commensal-specific T cells in epithelial regeneration[26,27], many of the transcripts upregulated in Th17 cells (TA) compared to Th1 cells (ID) were related to tissue repair, including *Tgfb1*, *Vegfa*, *Pdgfb*, *Furin*, *Mmp10*, *Mmp25* and *Areg*[26,28] (Figure 2A).

Of particular interest, Th17 cells isolated from the skin of *S. aureus*-associated mice (TA) expressed higher levels of transcripts related to neuronal interaction and regeneration, including *Neu3*, *Lif*, *Marveld1*, *Ramp1*, *Ramp3*, *Ccr4* and Tnfsf8, compared to Th1 cells (ID)[29–34] (Figure 2A). These signatures were also identified in the 3168 differentially expressed genes in Th17 (TA) compared to antigen-experienced cells (TEM) (Figures S2A and S2B).

The skin is densely innervated with sensory neurons that convey sensory information from the environment to the central nervous system[5,10,11]. Based on this, we next tracked the potential relationship of *S. aureus*-specific T cells with sensory neurons. To this end, SA1^{Tg} cells were transferred into mice engineered for sensory neuron visualization (alpha-CGRP^{+} reporter mice[35]). Mice were subsequently associated with *S. aureus* and imaged via intravital two-photon microscopy. Quantification of the distance between SA1^{Tg} T cells and nerve fibers over a defined period of intravital recording revealed that a fraction of SA1^{Tg} T cells were in direct contact or in close proximity to sensory neurons within the

dermis (<10 μm, 75%). Across all the time points assessed, *S. aureus*-specific T cells were significantly closer to alpha-CGRP$^+$ nerve fibers (mean±SEM, 5.9±0.2 μm) than to blood vessels (mean±SEM, 14±0.4 μm) (Figure 2B and Video S1). This contrasted with *S. aureus*-specific Th1 cells induced in the context of infection that were not associated with sensory neurons (Figure S2C). Thus, under steady state conditions, *S. aureus* topical association promotes accumulation of Th17 cells that colocalize with sensory neurons within the skin.

In the context of infection or injury, commensal-specific T cells can be recalled due to increased exposure to microbial antigens. Th17 cells exist in various configurations ranging from homeostatic to pathogenic that are characterized by defined core genes[36–38]. In line with alternative functions for commensal-specific T cells, Th17 cells induced following topical association showed a homeostatic transcriptomic profile, as opposed to a more pathogenic profile in Th17 cells induced by infection alone (ID) (Figures 2C, S2D and S2E). Functional enrichment analysis of Th17 cells recalled by infection post-association (TA+ID) compared to Th1 cells (ID) also showed an enrichment of three different GO terms related to nerve interaction and regeneration, more particularly, myeloid leukocyte activation (microglia regulation), regulation of cell projection-organization (axogenesis), and neurotransmitter transport (Figures 2C and 2D). In addition, seven other GO terms broadly related to tissue repair were also enriched in Th17 cells recalled by infection post-association (TA+ID) compared to Th1 cells (ID), including morphogenesis of an epithelium, ECM-receptor interaction, and response to wounding (Figure 2D). GO term enrichment for nerve interaction, regeneration and tissue repair were also confirmed when comparing recalled Th17 cells (TA+ID) to antigen-experienced cells (TEM) (Figure S2F).

Th17 cells recalled in the context of infection post-association (TA+ID) also expressed augmented levels of canonical Th17-associated genes along with multiple genes related to Th17 cell metabolism, including transporters (*Tmem176a* and *Tmem176b*)[39,40] compared to Th17 cells from TA or ID alone (Figures 2C–2F). Furthermore, Th17 cells recalled by infection of mice previously topically associated (TA+ID) expressed heightened levels of transcripts related to tissue repair and wound healing, as well as nerve interaction and regeneration (*Neu3*, *Ramp1*, *Lif*, *Ccr4*, *Tnfs8* and *Marveld1*), compared to Th17 from TA or ID alone (Figure 2F). Thus, Th17 cell responses induced by a commensal and subsequently recalled in the context of invasive infection express enhanced nerve interaction and regeneration gene signatures.

Staphylococcus aureus-elicited Th17 cells promote local nerve regeneration

To test the possibility that *S. aureus*-induced T cells could contribute to peripheral nerve regeneration, we next employed a model of skin injury that causes axonal damage[41]. In this model, the injured axons grow back to form a ring of nerve fibers surrounding the injury site (regeneration ring). Previous topical association with *S. aureus* increased the number of CD4$^+$ T cells (Figures 3A and 3B), and specifically Th17 cells accumulating at the periphery of the regeneration ring compared to unassociated mice (Figures S3A and S3B). Of note, topical association significantly increased the area and volume of the nerve fibers surrounding the injury site compared to unassociated mice, indicating enhanced

neuronal regeneration (Figures 3A and 3B). On the other hand, previous association with *S. epidermidis* (LM087) decreased fiber density upon injury compared to control, supporting the idea that defined strains and / or isolates of microbes may have different impact on neuronal repair (Figure S3C). To test the possibility that IL-17A could contribute to this phenomenon, we assessed neuronal regeneration in *S. aureus*-associated WT mice treated with anti-IL-17A blocking antibody and in *Il17a*$^{-/-}$ mice. Both approaches revealed that the ability of *S. aureus* to accelerate nerve regeneration post-injury was IL-17A-dependent (Figures 3C, 3D, S3D and S3E). Although IL-17A can be produced by numerous cell types within the skin, selective ablation of RORγt in T cells (Figure S1J) revealed that Th17 cells were required to support this process (Figures 3E and S3F). Altogether, these data indicate that *S. aureus*-specific Th17 cells are 1) in close proximity to dermal neurons, 2) enriched at the edge of injury site, and 3) can promote local nerve regeneration in an IL-17A-dependent manner.

Il17ra is upregulated by injured neurons and promotes nerve regeneration

Previous work demonstrated that, in *C. elegans*, an IL-17 ortholog could act directly on interneurons thereby regulating behavior[42]. IL-17RA expression by brain and enteric neurons also impact social behavior[43,44]. To assess the possibility that skin sensory neurons may also respond to IL-17A, we next isolated Dorsal Root Ganglion (DRG) sensory neurons. This population of neurons harbor axons that innervate the skin and also project to the spinal cord to convey sensory information to the central nervous system. Because dissection imposes strong damage to neuronal axons, cultured DRG neuronal cell bodies have been shown to be a relevant model to study neuronal injury and regeneration[45,46]. Therefore, we exposed DRG neurons isolated from WT mice to IL-17A *in vitro* (Figure 4A). After 24 hours IL-17A induced a discrete upregulation of seven genes and after 96 hours, 61 genes were differentially expressed between DRG treated with IL-17A versus vehicle control (Figure 4A). Notably, IL-17A promoted the expression of genes implicated in numerous aspects of neuronal maintenance and regeneration including neuronal development, migration, differentiation, and axon outgrowth (*Ccl11*, *Ccl2*, *Ereg*, *Mmp13*, *Il6*, *Mmp3*, *Fgf7* and *Cxcl5*) (Figure 4A)[47–52]. The second category of genes upregulated were related to neuronal response/function including neuronal excitation, synapses, and neuronal metabolism (*Steap4*, *Mme*, *Hsd11b1*, *Cxcl1*, *Prg4*, *Slc7a11* and *lgi2*) (Figure 4A). Downstream of IL-17A signaling, we also identified a group of genes related to antimicrobial defense including several members of the complement pathway (*C1ra*, *C3*, *C1s1*, *C1qtnf7* and *Cfb*) and antimicrobial peptide (*Lcn2)* (Figure 4A). Additionally, IL-17A promoted the expression of transcripts for MMPs and EGF (Figure 4A), both previously implicated in wound healing and keratinocyte differentiation[28]. Thus, IL-17A can directly signal to sensory neurons and induce a transcriptomic program related to neuronal and epithelial repair.

Previous work revealed that, following nerve injury, neurons undergo transcriptional reprogramming that requires the expression of the Activating transcription factor 3 (*Atf3*). This factor is upregulated rapidly after injury and promotes both axonal regeneration and functional recovery[53–55]. In our experimental system (Figure 4B), *Atf3* was specifically upregulated in cervical DRG2 neurons following punch biopsy (Figures 4C, 4D and

S4A). While DRG neurons expressed low levels of *Il17ra* at steady state, injury triggered significant upregulation of *Il17ra* that was sustained for at least 96 hours (Figure 4C and 4D). Of note, upregulation of *Atf3* and *Il17ra* followed a similar kinetic post-injury (Figure 4D). Injured neurons ($Atf3^{+}$) also expressed significantly more *Il17ra* than uninjured neurons ($Atf3^{-}$) (Figure 4E). Upregulation of *Il17ra* by lumbar DRG sensory neurons was also observed following sciatic nerve transection both at the mRNA (Figures 4F, 4G and S4B) and protein level (Figures 4F, 4H and S4C). Further, reanalysis of publicly available datasets[55] confirmed upregulation of *Il17ra* by injured neurons in a model of sciatic nerve transection (Figure S4D). Expression of *Il17ra* in neurons was significantly decreased in *Atf3*-deficient neurons post-injury[55] (Figures S4E and S4F) supporting a potential link between *Atf3* and the expression of *Il17ra.* Thus, upregulation of IL-17RA may be a conserved response to neuronal injury.

Next, to formally assess the contribution of direct IL-17A signaling on injured neurons to the repair process *in vivo*, we deleted *Il17ra* specifically in injured neurons ($Atf3^{Cre}Il17ra^{f/f}$). Using this approach, we confirmed that in mice previously associated with *S. aureus,* deletion of *Il17ra* in injured neurons significantly impaired nerve regeneration compared to controls (Figure S4G). Neuronal IL-17RA signaling promotes sensory neuron regeneration and is not associated with aberrant mechanical sensation.

As previously described[6,56], a fraction of cell bodies in the cervical DRG neurons were $Trpv1^{+}$ sensory neurons (Figure 5A). Following punch biopsy, we found that *Il17ra* expression was also enriched within $Trpv1^{+}$ neurons (Figure 5A). Expression of TRPV1 was not required for enhanced regeneration under these settings (Figure S5A).

Association with *S. aureus* increased neuronal regeneration post-injury, including both CGRP positive and negative fibers (Figure S5B). Notably, *S. aureus* association also increased the density of non-peptidergic sensory neurons stained with anti-GFRa-2 antibody, supporting the idea that this phenomenon may apply broadly to most C-fibers sensory neurons (Figure S5C). To formally assess the contribution of IL-17A signaling on sensory neurons to repair, we deleted *Il17ra* specifically in $TRPV1^{+}$ sensory neurons ($Trpv1^{Cre}Il17ra^{f/f}$). In mice previously associated with *S. aureus*, deletion of *Il17ra* in $TRPV1^{+}$ sensory neurons significantly impaired the regeneration of neuronal fibers (visualized with the pan neuronal marker β3-tubulin) compared to controls following punch biopsy (Figures 5B and 5C). Of particular interest, enhanced repair of sensory neurons (alpha-CGRP-expressing fibers) was completely abolished in the absence of IL-17RA (Figures 5B and 5D).

We next assessed the consequences of *S. aureus*-induced neuronal repair on pain sensation within the skin. Mechanosensation (mechanical allodynia) was assessed using the von Frey test. We observed a higher level of mechanical allodynia in associated-injured mice at seven days post-injury compared to naive and non-associated injured mice. Heightened mechanosensation was Th17 dependent (Figure 5E). We next assessed the long-term configuration of neuronal repair in mice previously associated with *S. aureus* or not. Of note, both associated and unassociated mice reached a comparable level of neuronal repair by day 30 (Figure S5D). In agreement with this observation, mice previously associated

with *S. aureus* did not display enhanced mechanical allodynia compared to control mice (Figure 5F), supporting the idea that accelerated repair did not come at the cost of sensory alteration. Altogether, these data suggest that, in response to the commensal microbiota, IL-17/IL-17RA axis regulates sensory nerve regeneration upon injury without impacting long-term mechanical sensation.

Discussion

Here, we uncover a previously unappreciated role for adaptive immunity in the direct control of neuronal repair in peripheral tissues. More particularly, we show that a locally acting cytokine released by tissue-resident commensal-specific T cells can coordinate neuronal repair within the skin.

Host behavior, metabolism, and inflammation can be profoundly influenced by the dialogue between the nervous and immune systems[57–60]. While most of our current understanding highlights innate immunity as a primary bridge between the immune and nervous systems, recent findings have uncovered a role for adaptive immunity in the control of host sensory processing and social behavior[44,61,62]. Quite remarkably, we found that adaptive immunity to the resident microbiota can also be repurposed to mediate neuronal repair.

Peripheral nervous system repair following injury requires the rapid activation of a regeneration program in damaged neurons in the context of a permissive environment mediated by various supporting cells[63]. Repair of the peripheral nervous system and reinnervation of tissues is of particular importance to restore sensory recovery, as well as to coordinate tissue reepithelization, neovascularization, and wound healing[14–16,64]. Failure to properly repair the peripheral nervous system can have dramatic consequences for the host including the development of neuropathic pain[65] and loss of both motor and sensory functions[66].

Previous work uncovered a fundamental role for macrophages and neutrophils in the restoration of neuronal integrity[41,67–71]. Within the skin, dermal macrophages surveil and shape the myelin sheath in nerve fibers, thereby contributing to axon sprouting upon mechanical injury[41]. Within the gut, muscularis macrophages induce neuronal protection and reduce the neuronal loss induced by infection via the β-2 adrenergic receptor[67]. Here we show that adaptive immunity can also contribute to this phenomenon.

Barrier tissues are constitutive targets of environmental stressors as well as primary sites of exposure to symbiotic and pathogenic microbes. Microbes at all barrier surfaces are actively recognized by the immune system, and encounters with symbiotic microbes promote the induction of cognate T cell responses and keratinocyte reepithelization after injury[26,27]. Since barrier tissues are defined by the constitutive coexistence with commensals and commensal-reactive tissue resident lymphocytes, any infection or injury occurs in the context of recall responses to the microbiota and more particularly Th17 cells. Our work propose that these canonical commensal-specific Th17 cells can act as major mediators of neuronal repair via IL-17A.

The mechanism underlying how IL-17A promotes neuronal repair remains to be fully investigated and may involve numerous pathways. For instance, we found that neuronal response to IL-17A promotes the production of factors that are able to communicate with both neuron and epithelium (e.g. *Fgf7*, *Mmp3*, *Mmp13*). Previous work demonstrated that somatosensory neurons undergo a conserved transcriptional reprogramming in response to a variety of nerve injuries, with the ATF3 at the core of neuronal reprogramming following injury[53,54,55]. Although the precise mechanism by which ATF3 coordinates these processes remains to fully understood, this transcription factor has been shown to promote axonal regeneration and repress cellular identity in injured neurons[55]. The roles of ATF3 in cell survival and maintenance also extend to other cellular types. For instance, upon stress, epithelial cells can induce ATF3 as a survival/healing-associated mitogenic mediator[72,73]. Our work reveals that the rapid upregulation of *Atf3* post-injury occurs in a concomitant manner with the expression of *Il17ra,* supporting the idea of a role for ATF3 in coordinating expression of IL-17RA in neurons. Expression of *Il17ra* was significantly reduced in injured neurons lacking *Atf3*[55] suggesting that *Il17ra* could be under the direct transcriptional control of ATF3, and that ATF3 may promote the acquisition of responsiveness to IL-17A by sensory neurons.

Our data also revealed that in addition to peptidergic sensory neurons ($CGRP^+$), other sensory fibers (non-peptidergic) also showed accelerated repair following *S. aureus* association, supporting the idea that IL-17A may broadly promote the repair of C-fiber sensory neurons. Although, accelerated repair did not come at the cost of long-term altered mechanical sensation, we could speculate that under highly inflammatory settings in which IL-17A is overrepresented the phenomenon we uncovered could also underlie heightened pain[74]. In support of this, psoriasis, an skin inflammatory disease, has been associated with both aberrant neuronal density and enhanced pain[75].

Restoration of tissue function and coordination of multisystem repair are of vital importance to the host and represent an extraordinary medical challenge. Exploration of the complex functions of immunity to the microbiota, our evolutionary partners, may provide therapeutic targets for these critical public health needs. In that context, our finding that upregulation of the IL-17A/IL-17RA axis represents a conserved response in injured neurons opens the door to therapeutic approaches to potentiate sensory recovery after injury, or limit neuropathies in the context of diabetes and chemotherapy.

Limitations of the study

This study proposes that IL-17A produced by commensal-specific Th17 cells directly signals sensory neurons following injury. However, more studies are required to assess if IL-17A alone is sufficient as a neurotrophic factor. Our work also propose that accelerated repair is not associated with altered pain sensation within the skin. A more thorough evaluation of other neuronal function (e.g. neuropeptide production, epigenetic alteration) would be important to perform. Finally, our work suggests that expression of IL-17RA may be downstream of ATF3 control, but additional work is required to formally address this point.

STAR Methods

RESOURCE AVAILABILITY

Lead contact—Further information and requests for resources and reagents should be directed to and will be fulfilled by the lead contact, Yasmine Belkaid (ybelkaid@niaid.nih.gov)

Materials availability—Reagents and mouse lines generated in this study are available upon signing a materials transfer agreement (MTA). All data are available in the main text or the supplementary materials.

Data and code availability

- Bulk RNA-seq data have been deposited at NCBI under accession numbers GSE196994, and are publicly available as of the date of publication. Accession numbers are listed in the key resources table. Microscopy data reported in this paper will be shared by the lead contact upon request.
- This paper does not report original code.
- Any additional information required to reanalyze the data reported in this paper is available from the lead contact upon request.

EXPERIMENTAL MODEL AND SUBJECT DETAILS

Mice—Conventional Specific Pathogen Free (SPF) wild-type C57BL/6, CD45.1 (B6.SJL-Ptprc^{a} Pepc^{b}/BoyJ), CD45.1.2 (C57BL/6J × B6.SJL-CD45^{a}(Ly5^{a})/Nai F1), *Rag1*$^{-/-}$ (BG.SJ L-CD45^{a}Ly5^{a}Nai-[KO] RAG 1), *Il17a*$^{-/-}$ (C57BL/6-[KO]IL17A), Foxp3GFP reporter (C57BL/6-Foxp3^{tm1Kuch}), *Il1r1*$^{-/-}$ (C57BL/6-[KO]IL1r1), and Albino B6 (C57BL/6NTac-*Tyr*^{tm1Arte}) mice were purchased from Taconic and maintained at NIAID animal facilities. *Lta*$^{-/-}$ (B6.129S2-*Lta*^{tm1Dch}/J), *Ox40*^{Cre} (B6.129X1(Cg)-*Tnfrsf4*$^{tm2(cre)Nik}$/J), *Rorc*$^{flox/flox}$ (B6(Cg)-*Rorc*^{tm3Litt}/J), *Trpv1*^{Cre} (B6.129-*Trpv1*$^{tm1(cre)Bbm}$/J), *Il17ra*$^{flox/flox}$ (B6.Cg-*Il17ra*$^{tm2.1Koll}$/J), *Il17a*^{Cre}(*Il17a*$^{tm1.1(icre)Stck}$/J) and ROSA-tdTomato (B6.Cg-*Gt(ROSA)26Sor*$^{tm14(CAG-tdTomato)Hze}$/J) mice were purchased from The Jackson Laboratories. *Atf3-IRES-Cre* mice[53] were kindly provided by Claire Le Pichon (*Eunice Kennedy Shriver* National Institute of Child Health and Human Development). Alpha-CGRP-GFP (Calca$^{tm1.1(EGFP/HBEGF)Mjz}$) mice were kindly provided by John O' Shea (National Institute of Arthritis and Musculoskeletal and Skin Diseases). *Il17ra*$^{-/-}$ were provided by Amgen. All mice were bred and maintained under specific pathogen-free conditions at an American Association for the Accreditation of Laboratory Animal Care (AAALAC)-accredited animal facility at the NIAID and housed in accordance with the procedures outlined in the Guide for the Care and Use of Laboratory Animals. All experiments were performed at the NIAID under an animal study proposal (LHIM-3E) approved by the NIAID Animal Care and Use Committee, except for DRG neuron related experiments that were performed in collaboration with Dr. Claire E. Le Pichon under an animal study proposal (20–003) approved by the *Eunice Kennedy Shriver* NICHD Animal Care and Use Committee. Mice were group housed (4–5 mice of same sex per cage) in a controlled environment with unrestricted access to water and standard chow diet. Mice

were randomly assigned to each experimental group. Unless otherwise noted, sex- and age-matched mice between 6 and 12 weeks of age were used for each experiment.

Bacterial strains—*Staphyloccocus aureus* (42F02, HV1043, NCTC8325ΔtarS, P6.34 and NCTC8325) was cultured in tryptic soy broth for 4 hours at 37°C with shaking at 200 rpm. *Staphyloccocus epidermidis* (LM087) was cultured for 18 hours in tryptic soy broth at 37°C.

DRG neuronal primary culture—Conventional Specific Pathogen Free (SPF) wild-type C57BL/6 mice (6–12 weeks old) were euthanized by CO_2 inhalation. Dorsal root ganglion (DRG) were dissected from all segments of the spinal cord of mice and transferred to neurobasal medium (Thermo Fisher) containing B-27 (Thermo Fisher) and penicillin/streptomycin (Thermo Fisher). DRGs were enzymatically dissociated by incubation in 2 mL of HEPES-buffered saline (Sigma) containing 1 mg/kg collagenase A (Sigma) and 2.4 U/ml dispase II (Roche Applied Sciences) for 40 min at 37°C. DMEM 10% FBS (Thermo Fisher) was added to the DRG suspension and the DRGs were allowed to settle to the bottom of the tube. The supernatant was removed and replaced with DMEM 10% FBS and cells were dissociated by triturating six times each through needles of decreasing diameter (18 G, 21 G, and 26 G) (Mckesson). Cells were resuspended in 3 ml of DMEM 10% FBS and overlayed on a 15% bovine serum albumin gradient (diluted in Neurobasal medium from a 30% BSA solution, Sigma) and centrifuged (260 g, 10 min). Supernatant and debris were removed, and the pellets of neuronal cells were resuspended in neurobasal medium. 5000 cells were seeded into flat-bottom 96-well plates coated with laminin (Thermo Fisher) and allowed to attach to the bottom of the wells for 2 hours, then the medium was removed and replaced with neurobasal medium containing 50 ng/μl nerve growth factor (Thermo Fisher). Culture medium was replaced daily for the duration of the experiment.

METHOD DETAILS

Topical association and infection—For commensal bacterial colonization (*S. aureus* and *S. epidermidis*), each mouse was topically associated by applying up to 5 mL of a culture of the specific bacteria (approximately 10^9 CFU/mL) across the entire skin surface, or by applying 1 mL on each ear skin, using a sterile cotton swab. Unless otherwise noted, associations were repeated every other day for a total of 4 times. For infections, mice were intradermally injected in the ear pinnae with 2×10^7 CFU of *S. aureus* (42F02), except for two-photon microscopy experiments (2×10^6 CFU).

Tissue processing for flow cytometry—Cell suspensions from skin-draining lymph nodes and ear skin were obtained as described previously[22,26,27,38]. Briefly, cells from lymph nodes were mashed through a 70 μm cell strainer to obtain cell suspensions. Ear pinna skin was split into the dorsal and the ventral sheets and placed in RPMI 1640 media supplemented with 2 mM L-glutamine, 1 mM sodium pyruvate, 1 mM non-essential amino acids, 50 μM β-mercaptoethanol, 20 mM HEPES, 100 U/ml of penicillin, 100 mg/ml of streptomycin, 0.5 mg/ml of DNAse I (Sigma-Aldrich) and 0.25 mg/ml of Liberase TL purified enzyme blend (Roche) for 90 minutes at 37°C and 5% CO_2. Digested ear skin sheets were homogenized using the Medicon/Medimachine tissue homogenizer system (Becton Dickinson).

T cell *in vitro* restimulation—For detection of basal cytokine potential, single-cell suspensions from various tissues were cultured directly *ex vivo* in a 96-well U-bottom plate in complete medium (RPMI 1640 supplemented with 10% fetal bovine serum, 2 mM L-glutamine, 1 mM sodium pyruvate, 1 mM non-essential amino acids, 20 mM HEPES, 100 U/ml penicillin, 100 mg/ml streptomycin, and 50 μM β-mercaptoethanol) and stimulated with 50 ng/ml of phorbol myristate acetate (PMA) (Sigma-Aldrich) and 5 mg/ml of ionomycin (Sigma-Aldrich) in the presence of brefeldin A (1:1000, GolgiPlug, BD Biosciences) for 150 minutes at 37°C in 5% CO_2. After stimulation, cells were assessed for intracellular cytokine production as described below.

Flow cytometry—Single cell suspensions were incubated with fluorochrome-conjugated antibodies against surface markers: CCR6 (29–2L17), CD3ε (145–2C11), CD4 (RM4–5), CD8β (eBioH35–17.2), CD11b (M1/70), CD11c (N418), CD19 (6D5), CD24 (M1/69), CD44 (IM7), CD45 (30-F11), CD45.1 (A20), CD45.2 (104), CD64 (X54–5/7.1), CD69 (H1.2F3), CD103 (2E7), Ly-6C (HK1.4), Ly-6G (1A8), MHCII (M5/114.15.2), TCRβ (H57–597), TCRγδ (GL-3), Vβ14 (14–2), Vβ8.1.2 (MR5–2), and intracellular markers: IFN-γ (XMG-1.2), IL-17A (eBio17B7), T-bet (ebio4B10), RORγt (B2D), Foxp3 (FJK-16s), GATA-3 (TWAJ) in PBS containing 20% of BD buffer for BUV brilliant fluorochromes for 20 minutes at 4°C and then washed. For cytokine and transcription factor intracellular staining, cells were fixed and permeabilized with the Foxp3/Transcription Factor Staining Buffer Set (eBioscience) and stained with fluorophore-conjugated antibodies for at least 60 minutes at 4°C. All staining were performed in the presence of purified anti-mouse CD16/32 (2.4G2, BioXcel). Dead cells were excluded from live samples using 4′,6-diamidino-2-phenylindol (DAPI; Sigma-Aldrich), whereas a LIVE/DEAD Fixable Blue Dead Cell Stain Kit (Invitrogen Life Technologies) was used in fixed samples. All antibodies were purchased from BD Biosciences, BioLegend, or eBioscience. Cells were acquired on BD Fortessa flow cytometer (BD Biosciences) running FACSDiva software (BD Biosciences), and data were analyzed by using FlowJo (v10, BD Biosciences).

Generation of *Staphylococcus aureus*-specific transgenic mice—Foxp3-GFP reporter mice were topically associated with *S. aureus* (42F02), and 4 weeks after the first association, mice were infected with *S. aureus* (42F02) by an intradermal injection in the ear to recall the *S. aureus*-specific T cells. To continue enriching the *S. aureus*-specific T cells, cell suspension obtained from the ear skin-draining lymph nodes was co-cultured with *S. aureus*-loaded dendritic cells for several weeks. FoxP3^{-}CD4^{+}CCR6^{+} T cells were FACSorted from the *in vitro* culture and subjected to single-cell sequencing of TCRα and TCRβ chains[76]. Clonal TCR pairs were identified and used in a hybridoma reconstitution screening assay to identify *S. aureus*-reactive TCR heterodimers. A single *S. aureus*-specific TCR pair was cloned into a hCD2-expression vector[77] and used to generate TCR-transgenic mice (SA1^{Tg}), to track *S. aureus*-specific T cells *in vivo*.

Adoptive transfer of *Staphylococcus aureus*-specific CD4 T cells—SA1^{Tg} mice were backcrossed to a CD45.1 *Rag1*$^{-/-}$ background to limit dual TCR expression and facilitate transferred cell identification. Unless otherwise noted, 0.5–1×10^{5} SA1^{Tg} CD4^{+} T

cells were transferred to CD45.2 recipient mice by intravenous injection in the tail vein one day before the first topical association or infection with *S. aureus* (42F02).

Antibody blockade—Naïve or *S. aureus*-associated WT mice were injected intraperitoneally with 0.5 mg of anti-IL-17A (17F3, BioXcell) or mouse IgG1 isotype control (MOPC-21, BioXcell). For protection experiments, mice received the antibody blockade treatment 2 days before the intradermal injection and then every other day until the takedown. For neuroregeneration experiments, mice received the antibody blockade treatment 2 days before the first round of associations and then every other day until the endpoint.

CFU quantification—CFU were determined as described before[78]. Briefly, samples were serially diluted with PBS in a 96-well plate, and 5 µl of each dilution was spotted 4 times in TSB agar (1 plate per sample, 20 µl per dilution). Plates were incubated at 37 °C overnight in a non-CO_2 incubator.

Hematoxylin and eosin histology—Mice were sacrificed seven days after the first topical association or intradermal infection with *S. aureus.* Mice associated with media TSB were used as controls. Ear skin was fixed in 10% PFA. Paraffin-embedded sections were cut at 0.5 mm, stained with hematoxylin and eosin, and examined histologically.

Bulk RNA-seq of *Staphylococcus aureus*-induced polyclonal T cells and bioinformatic analysis—T cells were FACsorted (BD FACS Aria, Becton Dickinson) from the skin-draining lymph nodes and ear skin tissues of Foxp3-GFP reporter mice. Mice were grouped based on the treatment received: unassociated (mice were associated with media TSB), topical association (mice received topical association with *S. aureus* (42F02) and were sacrificed 14 days after the first association), intradermal injection (mice were infected by intradermal injection with *S. aureus* (42F02) in the ear skin and sacrificed seven days later and recall (mice received topical association with *S. aureus* (42F02), 30 days after the first association they were infected by intradermal injection with *S. aureus* (42F02) and sacrificed seven days after the infection). Samples were stained with antibodies to MHCII, CD11b, CD11c, NK1.1, CD8α, γδTCR, CD49f, B220 and Fc Block (CD16/CD32) and 3 different populations of sorted cells analyzed were as follows: Th17 (Skin, Lineage$^-$CD45$^+$CD90.2$^+$TCRβ$^+$CD4$^+$Foxp3$^-$CCR6$^+$), Th1 (Skin, Lineage$^-$CD45$^+$CD90.2$^+$TCRβ$^+$CD4$^+$Foxp3$^-$CCR6$^-$) and TEM (Lymph node, Lineage$^-$CD45$^+$CD90.2$^+$TCRβ$^+$CD4$^+$Foxp3$^-$CD44^{high}CD62L^{low}). The RNA from the sorted T cells was extracted using the RNeasy Plus Micro Kit (Qiagen) as per manufacturer instructions. Libraries were prepared using the Clontech SMARTer Ultra low input mRNA-Seq sequence kit and samples were sequenced paired end (100bp per end) on a NextSeq550. For analysis, RNA-seq samples were mapped to the mm10 mouse genome with STAR[79]. Gene expression was assessed using HOMER's analyzeRepeats.pl with parameters rna, mm10, -count exons, -condenseGenes[80]. Differential gene expression was calculated using DESeq2[81]. Genes were considered differentially expressed with false discovery rate (FDR) < 0.05 and fold change (FC) > 2. Gene ontology analysis was done with Metascape (http://metascape.org)[82].

2-photon microscopy and quantification of *Staphylococcus aureus*-specific transgenic T cells- sensory neurons interaction—Albino alpha-CGRP-GFP reporter mice were transferred with $SA1^{Tg}$-RFP^{+} reporter cells and topically associated or intradermally infected with *S. aureus* (42F02) as described before. Prior to imaging, mice were injected with 25 μg of Alexa Fluor-647 labeled CD31 antibody (MEC13.3, BioLegend) retro-orbitally, in a total volume of 50 μL to visualize blood vessels. Intravital multiphoton microscopy was performed using Leica Mi8 DIVE (Deep In Vivo Explorer) inverted confocal microscope (Leica Microsystems) equipped with dual multiphoton lasers (Spectra Physics). Mai Tai DS was used for excitation of CGRP-GFP, and InSight DS for red and far-red probes. The microscope was additionally equipped with 4 ultra-sensitive HyD detectors, L 25.0 water-immersion objective (0.95 NA), a motorized stage, and Environmental Chamber (NIH Division of Scientific Equipment and Instrumentation Services) to maintain 37 °C for anesthetized animals. Mai Tai was tuned to 880 nm excitation, and InSight to 1150 nm excitation wavelengths. For non-invasive time-lapse imaging, tiled images of 2×2 fields were defined using Tilescan application of Leica Application Suite X (LAS X), and Z stacks consisting of 3–5 single planes (5–7 μm each over a total tissue depth of 30–50 μm) were acquired every 45 seconds for a total observation time between 1 to 6 hours. Raw imaging data were processed using Imaris (version 9.8.2, Bitplane). All imaging files were stabilized and adjusted for drifts prior to subsequent analysis. Cells ($SA1^{Tg}$) were surface-rendered using Imaris Surface module to generate 3D positional data at all time points. Peptidergic nerves (alpha-$CGRP^{+}$) and endothelia ($CD31^{+}$) were filament-rendered using Imaris Filament module, and then surface-rendered for all time points. The distances between the rendered T cell surfaces and the rendered nerve (or endothelium) surfaces were calculated using shortest distances (object-object) calculation module, and the data from all time points from all mice were collected and analyzed.

Neuroregeneration model, ear pinna skin confocal microscopy and image quantification—C57BL/6 mice were topically associated with *S. aureus* (42F02) and 21 days after the first association mice were topically associated again every day for four consecutive days. The day after the last association mice received a 1 mm ear punch. Mice were sacrificed for analysis 10 days after the punch biopsy. For ear skin whole mounts, ear skin was split into the ventral and dorsal sheets using fine forceps and the microscope. The ventral sheet with no cartilages was fixed in 1% paraformaldehyde solution (Electron Microscopy Sciences), overnight at 4°C with shaking. Tissues were blocked with 1% BSA, 0.25% Triton X-100 and Fc Block for 2 hours at RT with shaking. Tissues were first stained with β3-tubulin (TuJ-1, R & D System), CD4 (RM4–5, eBioscience), CD49f (eBioGoH3, eBioscience), alpha-CGRP (T-4032, Peninsula laboratories) and GFRa-2 (AF429, R & D System) in blocking solution overnight at 4 °C with shaking, washed with blocking solution (2x) and PBS (1x) for 60 minutes at RT with shaking and mounted with ProLong Gold (Molecular Probes) antifade reagent with the dermis facing the coverslip. Polyclonal goat anti-rabbit (Invitrogen) antibody was used as a secondary antibody to reveal alpha-CGRP staining and polyclonal rabbit anti-goat (Invitrogen) to reveal GFRa-2. Images were captured on a Leica TCS SP8 confocal microscope, equipped with HyD detectors and 40X oil objective (HC PL APO 40X/1.3 oil). Tiled images (7×7 up to 9×9), using a zoom of 1 and 3 μm slices were taken around the center of the ear punch with the full Z stack

(approximately 100–150 μm). Tiles and Z stacks were merged, and the area/volume of β3-tubulin/alpha-CGRP/GFRa-2 positive staining was batched for quantification. All analysis were done blinded. Using Imaris analysis software (version 9.8.2, Bitplane), a surface was drawn manually over the skin punch biopsy as well as the surrounding neuron-regenerative region. A mask was applied so that only the β3-tubulin signal in the nerve ring was present. A second surface was then applied onto the masked β3-tubulin channel to quantify the area/volume of neurons in the nerve ring around the punch. Similar approach was followed for alpha-CGRP and GFRa-2 quantification. For IL-17A$^+$ and CD4$^+$ T cell quantification, the "spots" feature was used to identify individual cells. Then, using the "spots close to surface" extension feature, we quantified the number of cells within 200 μm of the nerve ring using the surface that was drawn manually. Images were taken with the same parameters on the same experimental day for each independent experiment and the color threshold was set according to controls of each group and applied to all other samples to ensure comparability.

Dorsal root ganglia neurons culture stimulation with IL-17A—DRG neurons were seeded into flat-bottom 96-well plates coated with laminin (Thermo Fisher) and allowed to attach to the bottom of the wells for 2 hours, then the medium was removed and replaced with neurobasal medium containing 50 ng/μl nerve growth factor (Thermo Fisher). Following an overnight incubation, the supernatant was removed and replaced with neurobasal medium containing 50 ng/μl nerve growth factor, 10 mM cytosine arabinoside (Sigma), and 100 ng/ml IL-17A. Culture medium was replaced daily for the duration of the experiment. At the endpoint, the supernatant was removed, cells were lysed with RLT Plus buffer (Qiagen) and the RNA was extracted to perform bulk RNA-seq.

Cervical dorsal root ganglia extraction, RNAscope and image quantification—Mice were anesthetized by intraperitoneal injections of 1.2% Avertin. They were perfused with 10 mL PBS followed by 10 mL 4% PFA. Fur was removed, and the entire spinal column was dissected out by cutting once across the brain rostral to the cerebellum and once at the pelvis. The spinal column was briefly rinsed in PBS before laminectomy was performed to expose the spinal cord and dorsal root ganglia (DRG). Cervical DRGs 1–3 were dissected and placed directly into 4% PFA and post-fixed in 4% PFA overnight. After post-fixation, DRGs were placed in 30% sucrose overnight. Then, DRGs were placed in PBS and single DRGs were embedded in O.C.T compound (Tissue-Tek) and frozen on dry ice. Blocks were sectioned into 16 μm-thick slices onto positively charged slides using a Leica CM3050 S Research Cryostat. Slides were dried at 60°C for 10min, then stored at −80°C for up to two weeks. Multiplexed *in situ* hybridization was performed according to the manufacturer's instructions for fixed frozen sections (ACD: 323100, 323120), with minor changes (after sectioning, slides were not post-fixed in 4% PFA and the antigen retrieval steps were skipped). Probe targets (*Il17ra*, *Atf3*, *Trpv1* and *Tubb3*) were visualized using Opal dyes 520, 570, and 690 (Akoya). Image processing was performed using Imaris software package (version 9.8.2, Bitplane). The surface module and masking technique in combination with spots creation and channel arithmetic's was used to eliminate nonspecific signal and correcting cell nuclei for all samples. Cell module of Imaris was used to create 3D cell models specifically for neurons. We defined a neuron as a cell with one nucleus and a cytoplasm positive for *Tubb3*. Two groups of spots inside the neuron cytoplasm

were quantified using the fluorescence signal of *Il17ra*, *Atf3* and *Trpv1*. Number of spots, intensities and other statistical parameters were then exported, and statistical analysis was performed in Excel.

Sciatic nerve transection model and dorsal root ganglia confocal microscopy—Mice were anesthetized using 2% isoflurane and maintained at 1.5–1.8% isoflurane for the duration of the surgery. The left hindlimb was shaved and cleaned with 70% ethanol followed by betadine. A small incision was made in the skin in the middle of the thigh. Muscles were parted to reveal the sciatic nerve, which was then transected at the mid-thigh level. The overlaying muscle was placed back together, and the skin was held together with wound clips. After four days, lumbar DRG 3, 4 and 5 were extracted and fixed for 24 hours for RNAscope as described before, or 2 hours for confocal microscopy. DRG were embedded in OCT and sectioned as described before. Confocal microscopy on sectioned DRG were performed as previously described[54]. Briefly, fresh frozen sections were briefly washed in PBS followed, outlined with hydrophobic pen and permeabilized with PBS containing 0.1% Triton X (PBS-T). Sections were blocked in 10% normal goat serum in PBS for 1 hour at room temperature and incubated with primary antibodies (TuJ-1, R & D System; IL-17RA, Abcam) diluted in 10% normal goat serum in PBS-T overnight at 4°C. Slides were washed in PBS-T, then incubated in AF555 goat polyclonal anti-rabbit secondary antibodies (Invitrogen) in PBS-T for 2 hours at room temperature, followed by two washes in PBS-T. Slides were counter-stained with DAPI for 10 minutes at RT, washed two times with PBS-T and one time with PBS, and cover slipped with ProLong Gold (Molecular Probes) antifade reagent.

Footpad punch biopsy and von Frey test—Mice were topically associated with *S. aureus* (42F02) as described before, including the footpads. At day 25, mice received a 2 mm punch biopsy in each footpad. Behavioral experiments were done blind to genotype or treatment, seven days, or 28 days after punch biopsy. Mice were habituated for 30 min to inverted glass staining jars (10 cm long × 8.5 cm wide × 7 cm tall) placed on a wire mesh platform. White paper was placed between each chamber so the mice could not see each other. Only mice of the same sex were tested in the same session. Von Frey filaments were manually applied to the center of the mouse's hind paw. The following filaments were tested: 0.008, 0.02, 0.04, 0.07, 0.16, 0.4, 0.6, 1.0, 1.4 and 2 g. Testing was performed as described before[54]. Each animal received 10 stimulations with each filament. The inter trial interval was at least 15 s. If a mouse showed paw withdrawal responses or escape attempts for five trials or more out of 10, that filament force was considered its mechanical threshold. Once a mouse responded all 10 times to a given filament, no further testing of higher force filaments was performed, but they were scored as a 10/10 for graphing and analysis purposes.

QUANTIFICATION AND STATISTICAL ANALYSIS

Statistical analysis was performed using Prism v9.1 (GraphPad Software Inc., La Jolla, CA, USA). Statistical details of experiments can be found in figure legends.

Supplementary Material

Refer to Web version on PubMed Central for supplementary material.

Acknowledgments

This work was supported by the Division of Intramural Research of NIAID (1ZIAAI001132, 1ZIAAI001115, 1ZICAI001233 to YB), the Cancer Research Institute Irvington Postdoctoral Fellowship Program (ME), the Damon Runyon (WK), the intramural program at NICHD, ZIA-HD008966 (CELP) and the intramural program at NCCIH, ZIA-AT000028 (ATC). We thank Teresa Hawley (NIAID Flow Cytometry Core), Jinguo Chen and Galina Koroleva (NIH Center for Human Immunology), Juliana Perez-Chaparro (NIAID Microbiome Core), Kimberly Beacht and Ejae Lewis (NIAID Mucosal Immunology Section) and Parirokh Awasthi (NCI transgenic Mouse Model Laboratory) for technical support. We thank Biorender for providing professional templates for figures and graphical abstract.

Inclusion and diversity statement

One or more of the authors of this paper self-identifies as an underrepresented ethnic minority in their field of research or within their geographical location. One or more of the authors of this paper self-identifies as a gender minority in their field of research. One or more of the authors of this paper self-identifies as a member of the LGBTQIA+ community.

References

1. Ansaldo E, Farley TK, and Belkaid Y (2021). Control of Immunity by the Microbiota. Annu Rev Immunol 39, 449–479. 10.1146/ANNUREV-IMMUNOL-093019-112348. [PubMed: 33902310]
2. Naik S, Bouladoux N, Linehan JL, Han SJ, Harrison OJ, Wilhelm C, Conlan S, Himmelfarb S, Byrd AL, Deming C, et al. (2015). Commensal-dendritic-cell interaction specifies a unique protective skin immune signature. Nature 520, 104–108. 10.1038/NATURE14052. [PubMed: 25539086]
3. Linehan JL, Harrison OJ, Han SJ, Byrd AL, Vujkovic-Cvijin I, Villarino A. v., Sen SK, Shaik J, Smelkinson M, Tamoutounour S, et al. (2018). Non-classical Immunity Controls Microbiota Impact on Skin Immunity and Tissue Repair. Cell 172, 784–796.e18. 10.1016/j.cell.2017.12.033. [PubMed: 29358051]
4. Harrison OJ, Linehan JL, Shih H-Y, Bouladoux N, Han S-J, Smelkinson M, Sen SK, Byrd AL, Enamorado M, Yao C, et al. (2019). Commensal-specific T cell plasticity promotes rapid tissue adaptation to injury. Science (1979) 363. 10.1126/science.aat6280.
5. Blake KJ, Jiang XR, and Chiu IM (2019). Neuronal Regulation of Immunity in the Skin and Lungs. Trends Neurosci 42, 537–551. 10.1016/J.TINS.2019.05.005. [PubMed: 31213389]
6. Le Pichon CE, and Chesler AT (2014). The functional and anatomical dissection of somatosensory subpopulations using mouse genetics. Front Neuroanat 8. 10.3389/FNANA.2014.00021.
7. Mack MR, and Kim BS (2018). The Itch–Scratch Cycle: A Neuroimmune Perspective. Trends Immunol 39, 980–991. 10.1016/J.IT.2018.10.001. [PubMed: 30471983]
8. Oetjen LK, Mack MR, Feng J, Whelan TM, Niu H, Guo CJ, Chen S, Trier AM, Xu AZ, Tripathi S. v., et al. (2017). Sensory Neurons Co-opt Classical Immune Signaling Pathways to Mediate Chronic Itch. Cell 171, 217–228.e13. 10.1016/J.CELL.2017.08.006. [PubMed: 28890086]
9. Wang F, and Kim BS (2020). Itch: A Paradigm of Neuroimmune Crosstalk. Immunity 52, 753–766. 10.1016/J.IMMUNI.2020.04.008. [PubMed: 32433948]
10. Pinho-Ribeiro FA, and Chiu IM (2019). Nociceptor nerves set the stage for skin immunity. Cell Res 29, 877–878. 10.1038/s41422-019-0240-x. [PubMed: 31619764]
11. Udit S, Blake K, and Chiu IM (2022). Somatosensory and autonomic neuronal regulation of the immune response. Nat Rev Neurosci 23, 157–171. 10.1038/S41583-021-00555-4. [PubMed: 34997214]
12. Zhang S, Edwards TN, Chaudhri VK, Wu J, Cohen JA, Hirai T, Rittenhouse N, Schmitz EG, Zhou PY, McNeil BD, et al. (2021). Nonpeptidergic neurons suppress mast cells via glutamate

to maintain skin homeostasis. Cell 184, 2151–2166.e16. 10.1016/J.CELL.2021.03.002. [PubMed: 33765440]

13. Cohen JA, Wu J, and Kaplan DH (2020). Neuronal Regulation of Cutaneous Immunity. J Immunol 204, 264–270. 10.4049/JIMMUNOL.1901109. [PubMed: 31907268]
14. Barker AR, Rosson GD, and Dellon AL (2006). Wound healing in denervated tissue. Ann Plast Surg 57, 339–342. 10.1097/01.SAP.0000221465.69826.B7. [PubMed: 16929207]
15. Buckley G, Metcalfe AD, and Ferguson MWJ (2011). Peripheral nerve regeneration in the MRL/MpJ ear wound model. J Anat 218, 163–172. 10.1111/J.1469-7580.2010.01313.X. [PubMed: 20950365]
16. Wallengren J (1997). Vasoactive Peptides in the Skin. Journal of Investigative Dermatology Symposium Proceedings 2, 49–55. 10.1038/JIDSYMP.1997.11. [PubMed: 9487016]
17. Carvalho CR, Oliveira JM, and Reis RL (2019). Modern Trends for Peripheral Nerve Repair and Regeneration: Beyond the Hollow Nerve Guidance Conduit. Front Bioeng Biotechnol 7, 337. 10.3389/FBIOE.2019.00337/BIBTEX. [PubMed: 31824934]
18. Grice EA, and Segre JA (2011). The skin microbiome. Nat Rev Microbiol 9, 244–253. 10.1038/NRMICRO2537. [PubMed: 21407241]
19. Byrd AL, Belkaid Y, and Segre JA (2018). The human skin microbiome. Nature Reviews Microbiology 2018 16:3 16, 143–155. 10.1038/nrmicro.2017.157.
20. Tamoutounour S, Han SJ, Deckers J, Constantinides MG, Hurabielle C, Harrison OJ, Bouladoux N, Linehan JL, Link VM, Vujkovic-Cvijin I, et al. (2019). Keratinocyte-intrinsic MHCII expression controls microbiota-induced Th1 cell responses. Proc Natl Acad Sci U S A 116, 23643–23652. 10.1073/PNAS.1912432116/-/DCSUPPLEMENTAL. [PubMed: 31672911]
21. Naik S, Bouladoux N, Wilhelm C, Molloy MJ, Salcedo R, Kastenmuller W, Deming C, Quinones M, Koo L, Conlan S, et al. (2012). Compartmentalized control of skin immunity by resident commensals. Science 337, 1115–1119. 10.1126/SCIENCE.1225152. [PubMed: 22837383]
22. Constantinides MG, Link VM, Tamoutounour S, Wong AC, Perez-Chaparro PJ, Han SJ, Chen YE, Li K, Farhat S, Weckel A, et al. (2019). MAIT cells are imprinted by the microbiota in early life and promote tissue repair. Science 366, 494–499. 10.1126/SCIENCE.AAX6624. [PubMed: 31467190]
23. Byrd AL, Deming C, Cassidy SKB, Harrison OJ, Ng WI, Conlan S, Belkaid Y, Segre JA, and Kong HH (2017). Staphylococcus aureus and Staphylococcus epidermidis strain diversity underlying pediatric atopic dermatitis. Sci Transl Med 9. 10.1126/SCITRANSLMED.AAL4651/SUPPL_FILE/AAL4651_TABLES_S3_TO_S10.ZIP.
24. Liu H, Archer NK, Dillen CA, Stibitz S, Geha RS, and Miller Correspondence LS (2017). Staphylococcus aureus Epicutaneous Exposure Drives Skin Inflammation via IL-36-Mediated T Cell Responses. Cell Host Microbe 22, 653–666. 10.1016/j.chom.2017.10.006. [PubMed: 29120743]
25. Nakagawa S, Matsumoto M, Katayama Y, Oguma R, Wakabayashi S, Nygaard T, Saijo S, Inohara N, Otto M, Matsue H, et al. (2017). Staphylococcus aureus Virulent PSMα Peptides Induce Keratinocyte Alarmin Release to Orchestrate IL-17-Dependent Skin Inflammation. Cell Host Microbe 22, 667–677.e5. 10.1016/J.CHOM.2017.10.008. [PubMed: 29120744]
26. Linehan JL, Harrison OJ, Han S-J, Byrd AL, Vujkovic-Cvijin I, Villarino A.v, Sen SK, Shaik J, Smelkinson M, Tamoutounour S, et al. (2018). Non-classical immunity controls microbiota impact on skin immunity and tissue repair HHS Public Access. Cell 172, 784–796. 10.1016/j.cell.2017.12.033. [PubMed: 29358051]
27. Harrison OJ, Linehan JL, Shih HY, Bouladoux N, Han SJ, Smelkinson M, Sen SK, Byrd AL, Enamorado M, Yao C, et al. (2019). Commensal-specific T cell plasticity promotes rapid tissue adaptation to injury. Science 363. 10.1126/SCIENCE.AAT6280.
28. Werner S, and Grose R (2003). Regulation of wound healing by growth factors and cytokines. Physiol Rev 83, 835–870. 10.1152/PHYSREV.2003.83.3.835. [PubMed: 12843410]
29. Kappagantula S, Andrews MR, Cheah M, Abad-Rodriguez J, Dotti CG, and Fawcett JW (2014). Neu3 sialidase-mediated ganglioside conversion is necessary for axon regeneration and is blocked in CNS axons. The Journal of neuroscience 34, 2477–2492. 10.1523/JNEUROSCI.4432-13.2014. [PubMed: 24523539]

30. Oshima K, Teo DTW, Senn P, Starlinger V, and Heller S (2007). LIF promotes neurogenesis and maintains neural precursors in cell populations derived from spiral ganglion stem cells. BMC Dev Biol 7. 10.1186/1471-213X-7-112.

31. Pitman M, Emery B, Binder M, Wang S, Butzkueven H, and Kilpatrick TJ (2004). LIF receptor signaling modulates neural stem cell renewal. Mol Cell Neurosci 27, 255–266. 10.1016/J.MCN.2004.07.004. [PubMed: 15519241]

32. Bauer S, and Patterson PH (2006). Leukemia inhibitory factor promotes neural stem cell self-renewal in the adult brain. J Neurosci 26, 12089–12099. 10.1523/JNEUROSCI.3047-06.2006. [PubMed: 17108182]

33. Liu W, Han F, Qu S, Yao Y, Zhao J, Akhtar ML, Ci Y, Zhang H, Li H, Zhao Y, et al. (2018). MARVELD1 depletion leads to dysfunction of motor and cognition via regulating glia-dependent neuronal migration during brain development. Cell Death Dis 9. 10.1038/S41419-018-1027-6.

34. Kwon MJ, Shin HY, Cui Y, Kim H, le Thi AH, Choi JY, Kim EY, Hwang DH, and Kim BG (2015). CCL2 Mediates Neuron–Macrophage Interactions to Drive Proregenerative Macrophage Activation Following Preconditioning Injury. Journal of Neuroscience 35, 15934–15947. 10.1523/JNEUROSCI.1924-15.2015. [PubMed: 26631474]

35. Nagashima H, Mahlakõiv T, Shih HY, Davis FP, Meylan F, Huang Y, Harrison OJ, Yao C, Mikami Y, Urban JF, et al. (2019). Neuropeptide CGRP Limits Group 2 Innate Lymphoid Cell Responses and Constrains Type 2 Inflammation. Immunity 51, 682–695.e6. 10.1016/J.IMMUNI.2019.06.009. [PubMed: 31353223]

36. Lee Y, Awasthi A, Yosef N, Quintana FJ, Xiao S, Peters A, Wu C, Kleinewietfeld M, Kunder S, Hafler DA, et al. (2012). Induction and molecular signature of pathogenic TH17 cells. Nat Immunol 13, 991–999. 10.1038/NI.2416. [PubMed: 22961052]

37. Lee JY, Hall JA, Kroehling L, Wu L, Najar T, Nguyen HH, Lin WY, Yeung ST, Silva HM, Li D, et al. (2020). Serum Amyloid A Proteins Induce Pathogenic Th17 Cells and Promote Inflammatory Disease. Cell 180, 79–91.e16. 10.1016/J.CELL.2019.11.026. [PubMed: 31866067]

38. Lim AI, McFadden T, Link VM, Han SJ, Karlsson RM, Stacy A, Farley TK, Lima-Junior DS, Harrison OJ, Desai J. v., et al. (2021). Prenatal maternal infection promotes tissue-specific immunity and inflammation in offspring. Science (1979) 373. 10.1126/SCIENCE.ABF3002.

39. Ciofani M, Madar A, Galan C, Sellars M, MacE K, Pauli F, Agarwal A, Huang W, Parkurst CN, Muratet M, et al. (2012). A validated regulatory network for Th17 cell specification. Cell 151, 289. 10.1016/J.CELL.2012.09.016. [PubMed: 23021777]

40. Drujont L, Lemoine A, Moreau A, Bienvenu G, Lancien M, Cens T, Guillot F, Beriou G, Bouchet-Delbos L, Fehling HJ, et al. (2016). RORγt+ cells selectively express redundant cation channels linked to the Golgi apparatus. Scientific Reports 2016 6:1 6, 1–13. 10.1038/srep23682.

41. Kolter J, Feuerstein R, Zeis P, Hagemeyer N, Paterson N, d'Errico P, Baasch S, Amann L, Masuda T, Lösslein A, et al. (2019). A Subset of Skin Macrophages Contributes to the Surveillance and Regeneration of Local Nerves. Immunity 50, 1482–1497.e7. 10.1016/J.IMMUNI.2019.05.009. [PubMed: 31201094]

42. Chen C, Itakura E, Nelson GM, Sheng M, Laurent P, Fenk LA, Butcher RA, Hegde RS, and de Bono M (2017). IL-17 is a neuromodulator of Caenorhabditis elegans sensory responses. Nature 2016 542:7639 542, 43–48. 10.1038/nature20818.

43. Reed MD, Yim YS, Wimmer RD, Kim H, Ryu C, Welch GM, Andina M, King HO, Waisman A, Halassa MM, et al. (2020). IL-17a promotes sociability in mouse models of neurodevelopmental disorders. Nature | 577. 10.1038/s41586-019-1843-6.

44. Leonardi I, Gao IH, Lin W-Y, and Johncilla M (2022). Mucosal fungi promote gut barrier function and social behavior via Type 17 immunity. Cell 185, 1–16. 10.1016/j.cell.2022.01.017. [PubMed: 34995512]

45. Melli G, and Höke A (2009). Dorsal Root Ganglia Sensory Neuronal Cultures: a tool for drug discovery for peripheral neuropathies. Expert Opin Drug Discov 4, 1035. 10.1517/17460440903266829. [PubMed: 20657751]

46. Saijilafu, and Zhou FQ (2012). Genetic Study of Axon Regeneration with Cultured Adult Dorsal Root Ganglion Neurons. J Vis Exp. 10.3791/4141.

47. Dordoe C, Chen K, Huang W, Chen J, Hu J, Wang X, and Lin L (2021). Roles of Fibroblast Growth Factors and Their Therapeutic Potential in Treatment of Ischemic Stroke. Front Pharmacol 12. 10.3389/FPHAR.2021.671131.
48. Liu YF, Liang JJ, Ng TK, Hu Z, Xu C, Chen S, Chen SL, Xu Y, Zhuang X, Huang S, et al. (2021). CXCL5/CXCR2 modulates inflammation-mediated neural repair after optic nerve injury. Exp Neurol 341. 10.1016/J.EXPNEUROL.2021.113711.
49. Kummer KK, Zeidler M, Kalpachidou T, and Kress M (2021). Role of IL-6 in the regulation of neuronal development, survival and function. Cytokine 144, 155582. 10.1016/J.CYTO.2021.155582. [PubMed: 34058569]
50. Zhan L, Zheng L, Hosoi T, Okuma Y, and Nomura Y (2015). Stress-Induced Neuroprotective Effects of Epiregulin and Amphiregulin. PLoS One 10. 10.1371/JOURNAL.PONE.0118280.
51. Eugenin EA, D'Aversa TG, Lopez L, Calderon TM, and Berman JW (2003). MCP-1 (CCL2) protects human neurons and astrocytes from NMDA or HIV-tat-induced apoptosis. J Neurochem 85, 1299–1311. 10.1046/J.1471-4159.2003.01775.X. [PubMed: 12753088]
52. Wang F, Baba N, Shen Y, Yamashita T, Tsuru E, Tsuda M, Maeda N, and Sagara Y (2017). CCL11 promotes migration and proliferation of mouse neural progenitor cells. Stem Cell Res Ther 8, 1–11. 10.1186/S13287-017-0474-9/FIGURES/5. [PubMed: 28057078]
53. Nguyen MQ, Le Pichon CE, and Ryba N (2019). Stereotyped transcriptomic transformation of somatosensory neurons in response to injury. Elife 8. 10.7554/ELIFE.49679.
54. Wlaschin JJ, Gluski JM, Nguyen E, Silberberg H, Thompson JH, Chesler AT, and Le Pichon CE (2018). Dual leucine zipper kinase is required for mechanical allodynia and microgliosis after nerve injury. Elife 7. 10.7554/ELIFE.33910.
55. Renthal W, Tochitsky I, Yang L, Cheng Y-C, Li E, Kawaguchi R, Geschwind DH, and Woolf CJ (2020). Transcriptional reprogramming of distinct peripheral sensory neuron subtypes after axonal injury HHS Public Access. Neuron 108, 128–144. 10.1016/j.neuron.2020.07.026. [PubMed: 32810432]
56. Cavanaugh DJ, Chesler AT, Jackson AC, Sigal YM, Yamanaka H, Grant R, O'Donnell D, Nicoll RA, Shah NM, Julius D, et al. (2011). Trpv1 Reporter Mice Reveal Highly Restricted Brain Distribution and Functional Expression in Arteriolar Smooth Muscle Cells. The Journal of Neuroscience 31, 5067. 10.1523/JNEUROSCI.6451-10.2011. [PubMed: 21451044]
57. Rankin LC, and Artis D (2018). Beyond Host Defense: Emerging Functions of the Immune System in Regulating Complex Tissue Physiology. Cell 173, 554–567. 10.1016/J.CELL.2018.03.013. [PubMed: 29677509]
58. Kabata H, and Artis D (2019). Neuro-immune crosstalk and allergic inflammation. J Clin Invest 129, 1475–1482. 10.1172/JCI124609. [PubMed: 30829650]
59. Chu C, Artis D, and Chiu IM (2020). Neuro-immune Interactions in the Tissues. Immunity 52, 464–474. 10.1016/J.IMMUNI.2020.02.017. [PubMed: 32187517]
60. Saloman JL, Cohen JA, and Kaplan DH (2020). Intimate neuro-immune interactions: breaking barriers between systems to make meaningful progress. Curr Opin Neurobiol 62, 60–67. 10.1016/J.CONB.2019.11.021. [PubMed: 31841783]
61. Herz J, Fu Z, Kim K, Dykstra T, Wall M, Li H, Salvador AF, Zou B, Yan N, Blackburn SM, et al. (2021). GABAergic neuronal IL-4R mediates T cell effect on memory. Neuron 109, 3609–3618.e9. 10.1016/J.NEURON.2021.10.022. [PubMed: 34793707]
62. Choi GB, Yim YS, Wong H, Kim S, Kim H, Kim S. v, Hoeffer CA, Littman DR, and Huh JR (2016). The maternal interleukin-17a pathway in mice promotes autismlike phenotypes in offspring HHS Public Access. Science (1979) 351, 933–939. 10.1126/science.aad0314.
63. Eric Huebner SA, and Strittmatter SM (2010). Axon Regeneration in the Peripheral and Central Nervous. Results Probl Cell Differ 48, 339–351. 10.1007/400_2009_19.
64. Buckley G, Wong J, Metcalfe AD, and Ferguson MWJ (2012). Denervation affects regenerative responses in MRL/MpJ and repair in C57BL/6 ear wounds. J Anat 220, 3–12. 10.1111/J.1469-7580.2011.01452.X. [PubMed: 22066944]
65. Costigan M, Scholz J, and Woolf CJ (2009). Neuropathic Pain: A Maladaptive Response of the Nervous System to Damage. 10.1146/annurev.neuro.051508.135531 32, 1–32. 10.1146/ANNUREV.NEURO.051508.135531.

66. Navarro X, Geuna S, Grothe C, and Haastert-Talini K (2018). Introduction: Thematic Papers Issue on Peripheral Nerve Regeneration and Repair. Anat Rec 301, 1614–1617. 10.1002/AR.23941.

67. Ahrends T, Aydin B, Matheis F, Classon CH, Marchildon F, Furtado GC, Lira SA, and Mucida D (2021). Enteric pathogens induce tissue tolerance and prevent neuronal loss from subsequent infections. Cell 184, 5715–5727.e12. 10.1016/J.CELL.2021.10.004. [PubMed: 34717799]

68. Matheis F, Muller PA, Graves CL, Gabanyi I, Kerner ZJ, Costa-Borges D, Ahrends T, Rosenstiel P, and Mucida D (2020). Adrenergic Signaling in Muscularis Macrophages Limits Infection-Induced Neuronal Loss. Cell 180, 64–78.e16. 10.1016/J.CELL.2019.12.002. [PubMed: 31923400]

69. McGettrick HM (2021). Bridging the gap—Immune cells that can repair nerves. Cellular & Molecular Immunology 2021 18:4 18, 784–786. 10.1038/s41423-021-00642-7.

70. Sas AR, Carbajal KS, Jerome AD, Menon R, Yoon C, Kalinski AL, Giger RJ, and Segal BM (2020). A new neutrophil subset promotes CNS neuron survival and axon regeneration. Nature Immunology 2020 21:12 21, 1496–1505. 10.1038/s41590-020-00813-0.

71. Cattin AL, Burden JJ, van Emmenis L, MacKenzie FE, Hoving JJA, Garcia Calavia N, Guo Y, McLaughlin M, Rosenberg LH, Quereda V, et al. (2015). Macrophage-Induced Blood Vessels Guide Schwann Cell-Mediated Regeneration of Peripheral Nerves. Cell 162, 1127. 10.1016/J.CELL.2015.07.021. [PubMed: 26279190]

72. Harper EG, Alvares SM, and Carter WG (2005). Wounding activates p38 map kinase and activation transcription factor 3 in leading keratinocytes. J Cell Sci 118, 3471–3485. 10.1242/JCS.02475. [PubMed: 16079289]

73. Yang H, Park SH, Choi HJ, and Moon Y (2009). Epithelial cell survival by activating transcription factor 3 (ATF3) in response to chemical ribosome-inactivating stress. Biochem Pharmacol 77, 1105–1115. 10.1016/J.BCP.2008.11.028. [PubMed: 19101521]

74. Jiang X, Zhou R, Zhang Y, Zhu T, Li Q, and Zhang W (2022). Interleukin-17 as a potential therapeutic target for chronic pain. Front Immunol 13. 10.3389/FIMMU.2022.999407.

75. Misery L, Shourick J, and Taieb C (2020). Skin pain and psoriasis. J Am Acad Dermatol 83, 245–246. 10.1016/J.JAAD.2019.12.066. [PubMed: 31931087]

76. Dash P, McClaren JL, Oguin TH, Rothwell W, Todd B, Morris MY, Becksfort J, Reynolds C, Brown SA, Doherty PC, et al. (2011). Paired analysis of TCRα and TCRβ chains at the single-cell level in mice. J Clin Invest 121, 288–295. 10.1172/JCI44752. [PubMed: 21135507]

77. Sun G, Liu X, Mercado P, Jenkinson SR, Kypriotou M, Feigenbaum L, Galéra P, and Bosselut R (2005). The zinc finger protein cKrox directs CD4 lineage differentiation during intrathymic T cell positive selection. Nat Immunol 6, 373–381. 10.1038/NI1183. [PubMed: 15750595]

78. Stacy A, Andrade-Oliveira V, McCulloch JA, Hild B, Oh JH, Perez-Chaparro PJ, Sim CK, Lim AI, Link VM, Enamorado M, et al. (2021). Infection trains the host for microbiota-enhanced resistance to pathogens. Cell 184, 615–627.e17. 10.1016/J.CELL.2020.12.011. [PubMed: 33453153]

79. Dobin A, Davis CA, Schlesinger F, Drenkow J, Zaleski C, Jha S, Batut P, Chaisson M, and Gingeras TR (2013). STAR: ultrafast universal RNA-seq aligner. Bioinformatics 29, 15–21. 10.1093/BIOINFORMATICS/BTS635. [PubMed: 23104886]

80. Heinz S, Benner C, Spann N, Bertolino E, Lin YC, Laslo P, Cheng JX, Murre C, Singh H, and Glass CK (2010). Simple combinations of lineage-determining transcription factors prime cis-regulatory elements required for macrophage and B cell identities. Mol Cell 38, 576–589. 10.1016/J.MOLCEL.2010.05.004. [PubMed: 20513432]

81. Love MI, Huber W, and Anders S (2014). Moderated estimation of fold change and dispersion for RNA-seq data with DESeq2. Genome Biol 15, 1–21. 10.1186/S13059-014-0550-8/FIGURES/9.

82. Zhou Y, Zhou B, Pache L, Chang M, Khodabakhshi AH, Tanaseichuk O, Benner C, and Chanda SK (2019). Metascape provides a biologist-oriented resource for the analysis of systems-level datasets. Nat Commun 10. 10.1038/S41467-019-09234-6.

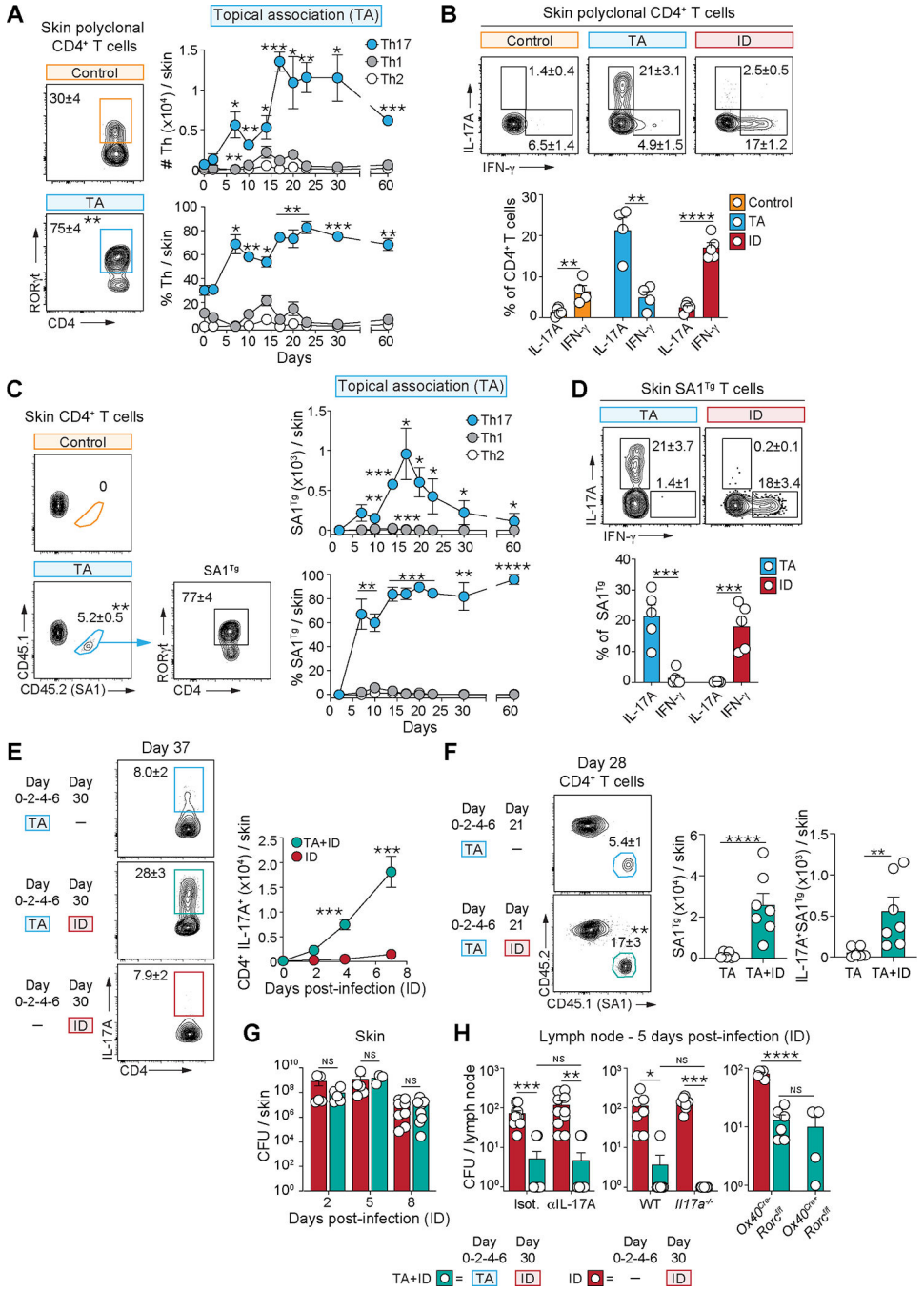

Figure 1. Staphylococcus aureus colonization induces Th17 cells that have no impact on host protection

(A) Mice were topically associated (TA) with *S. aureus*. RORγt expression by skin CD4$^+$ T cells at two weeks post-association (left). Absolute numbers and frequencies of Th17 (RORγt$^+$CD4$^+$Foxp3$^-$), Th1 (T-bet$^+$CD4$^+$Foxp3$^-$) and Th2 (Gata3$^+$CD4$^+$Foxp3) cells in the skin (right).

(B) Mice were topically associated (TA) or intradermally injected (ID) with *S. aureus*. IL-17A and IFN-γ production by skin $CD4^+$ T cells (top), two weeks post-association. Frequency quantification (bottom).
(C) Mice were transferred with *S. aureus*-specific TCR-transgenic $CD4^+$ T cells ($SA1^{Tg}$) and topically associated (TA) with *S. aureus*. RORγt expression by $SA1^{Tg}$ cells in the ear skin, two weeks after the first association (left). Absolute numbers and frequencies of $SA1^{Tg}$ Th17 ($ROR\gamma t^+CD4^+Foxp3^-$), Th1 ($T\text{-}bet^+CD4^+Foxp3^-$) and Th2 ($Gata3^+CD4^+Foxp3^-$) cells (right).
(D) Contour plots (top) and frequency quantification (bottom) of IL-17A and IFN-γ production by $SA1^{Tg}$ cells in the skin, two weeks post-association.
(E) Mice previously associated (TA) with *S. aureus* were infected with the same strain by intradermal injection (ID). IL-17A production by $CD4^+$ T cells in the ear skin, seven days post-infection (left). Absolute numbers of $IL\text{-}17A^+CD4^+$ T cells (right).
(F) Mice previously transferred with $SA1^{Tg}$ and topically associated (TA) with *S. aureus* were infected with the same strain by intradermal injection (ID). Frequency of $SA1^{Tg}$ cells in the skin, seven days post-infection (left). Absolute numbers of IL-17A production by $SA1^{Tg}$ cells (right).
(G-H) Previously associated (TA) mice with *S. aureus* were infected with the same strain by intradermal injection (ID). (**G)** CFU in the skin of WT mice. (**H)** CFU in the skin-draining lymph nodes of mice treated with anti-IL-17A blocking (αIL-17A) antibody or isotype (Isot.) control (left), *Il17a*$^{-/-}$ mice (middle), Th17 deficient mice (*Ox40*$^{Cre+}$*Rorc*$^{f/f}$) (right). Numbers in contour plots, kinetic curve graphs and bar plots indicate means ± SEM. Each dot represents an individual mouse (B, D, F, G and H). Data represent at least two experiments with three to eight mice per group. *$p < 0.05$, **$p < 0.01$, ***$p < 0.001$, and ****$p < 0.0001$ and “NS”, not significant as calculated with Student’s t test. See also Figure S1.

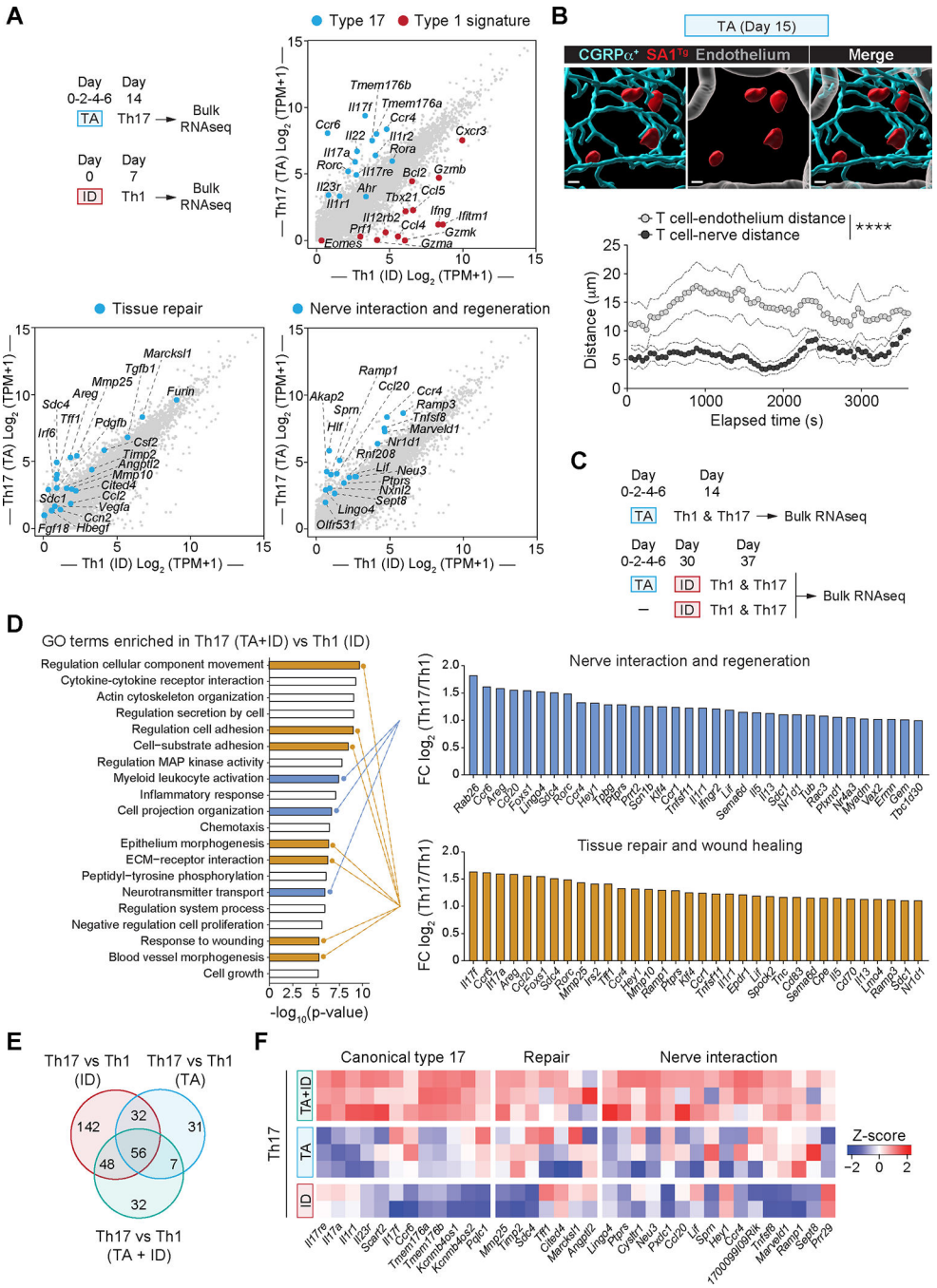

Figure 2. *Staphylococcus aureus*-induced T cells express a neuronal regeneration transcriptomic signature.

(A) Th17 ($CCR6^{+}CD4^{+}Foxp3^{-}$) cells from the skin of topically associated (TA) mice and Th1 ($CCR6^{-}CD4^{+}Foxp3^{-}$) cells from the skin of intradermally infected (ID) mice were sorted for bulk RNA-seq analysis. Scatter plots highlighting differentially expressed genes comparing Th17 (TA) versus Th1 (ID) cells for type 1 and type 17 signature (top right), tissue repair (bottom left) and nerve interaction and regeneration (bottom right).

(B) alpha-CGRP-GFP nerve reporter mice were transferred with $SA1^{Tg}$-RFP^{+} and topically associated (TA) with *S. aureus*. Ear pinnae skin was assessed by 2-photon microscopy two weeks after first association. Frame from video reconstruction (top) showing the close interaction between $SA1^{Tg}$ cells (red) and alpha-$CGRP^{+}$ nerve fibers (cyan). Scale bar (10 μm). Quantification (bottom) of the shortest distances of the $SA1^{Tg}$ cells from the $CGRP^{+}$ nerve fibers compared with the shortest distances from the blood vessels (gray, stained with anti-CD31).

(C) Mice previously associated with *S. aureus* were infected with the same strain by intradermal injection. This recall group (TA+ID) was compared to mice that received only topical association (TA) or only intradermal injection (ID). Th17 ($CCR6^{+}CD4^{+}Foxp3^{-}$) and Th1 ($CCR6^{-}CD4^{+}Foxp3^{-}$) cells within the ear skin were simultaneously sorted in each of the three groups for transcriptomic analysis.

(D) Top 20 GO terms enriched in Th17 (recall TA+ID) versus Th1 (ID) cells (left). Top 34 genes enriched in Th17 cells related to nerve interaction and regeneration (top right) and tissue repair and wound healing (bottom right).

(E) Venn diagram showing the number of up-regulated genes in Th17 cells compared to Th1 cells within each treatment (intradermal infection (ID), topical association (TA), recall (TA+ID)).

(F) Heatmap showing the relative expression of genes from the Th17 transcriptomic core set defined in figure 2E.

In A and C-F, pools of 40 (TA), 15 (ID) and 10 (TA+ID) mice per group were used. Data in B shows one representative video out of four videos taken in four independent mice and independent experiments. ****$p < 0.0001$ as calculated with Student's t test. See also Figure S2, and Video S1.

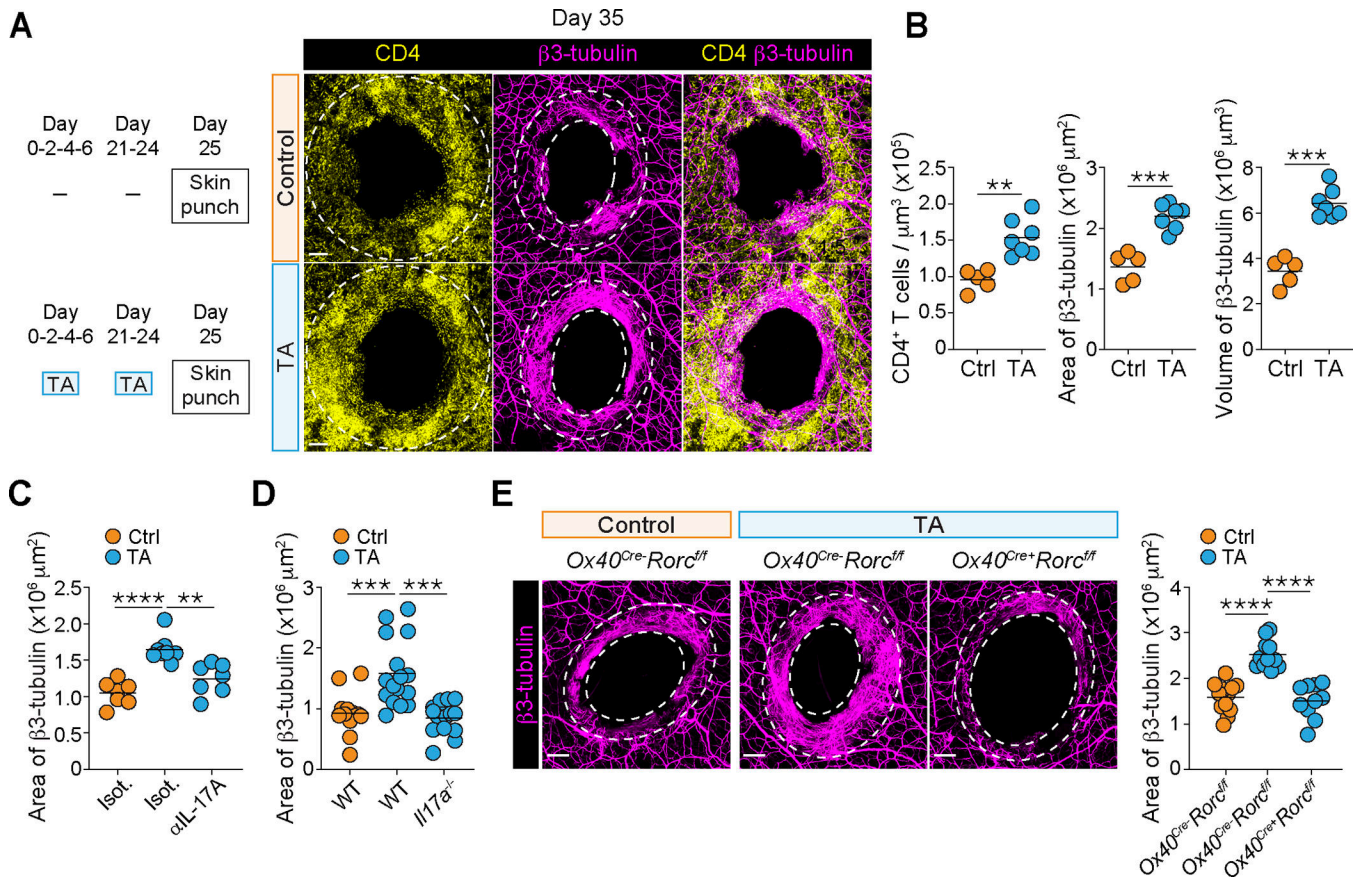

Figure 3. *Staphylococcus aureus*-elicited Th17 cells promote local nerve regeneration.

(A to **E)** Mice received (or not) two rounds of topical association (TA) with *S. aureus*. Subsequently ear pinnae were injured by punch biopsy and analyzed by confocal microscopy, 10 days after punch. (**A)** Confocal images of the ring of nerve regeneration (β3-tubulin) and $CD4^+$ T cell infiltration around the injured site, in unassociated (Ctrl) and associated mice (TA). (**B)** Quantification of the absolute numbers of $CD4^+$ T cells, area, and volume of the pan β3-tubulin nerve fibers, around the injured site. (**C)** Quantification of area of the nerve regeneration ring in unassociated (Ctrl) and associated mice (TA) treated with anti-IL-17A blocking antibody (αIL-17A) or isotype control (Isot.) and, (**D)** WT and *Il17a*$^{-/-}$ mice. (**E)** Confocal images (left); and quantification (right) of the area of the nerve regeneration ring, in unassociated (Ctrl) and associated (TA) WT (*Ox40*$^{Cre-}$*Rorc*$^{f/f}$) and Th17-deficient (*Ox40*$^{Cre+}$*Rorc*$^{f/f}$) mice. Scale bars (200 µm).

Dot plots show means, and each dot represents an individual mouse. D is a pool of two independent experiment. Data represent at least two experiments with 5–12 mice per group. *p < 0.05, **p < 0.01, ***p < 0.001, and ****p < 0.0001 as calculated with Student's t test. See also Figure S3.

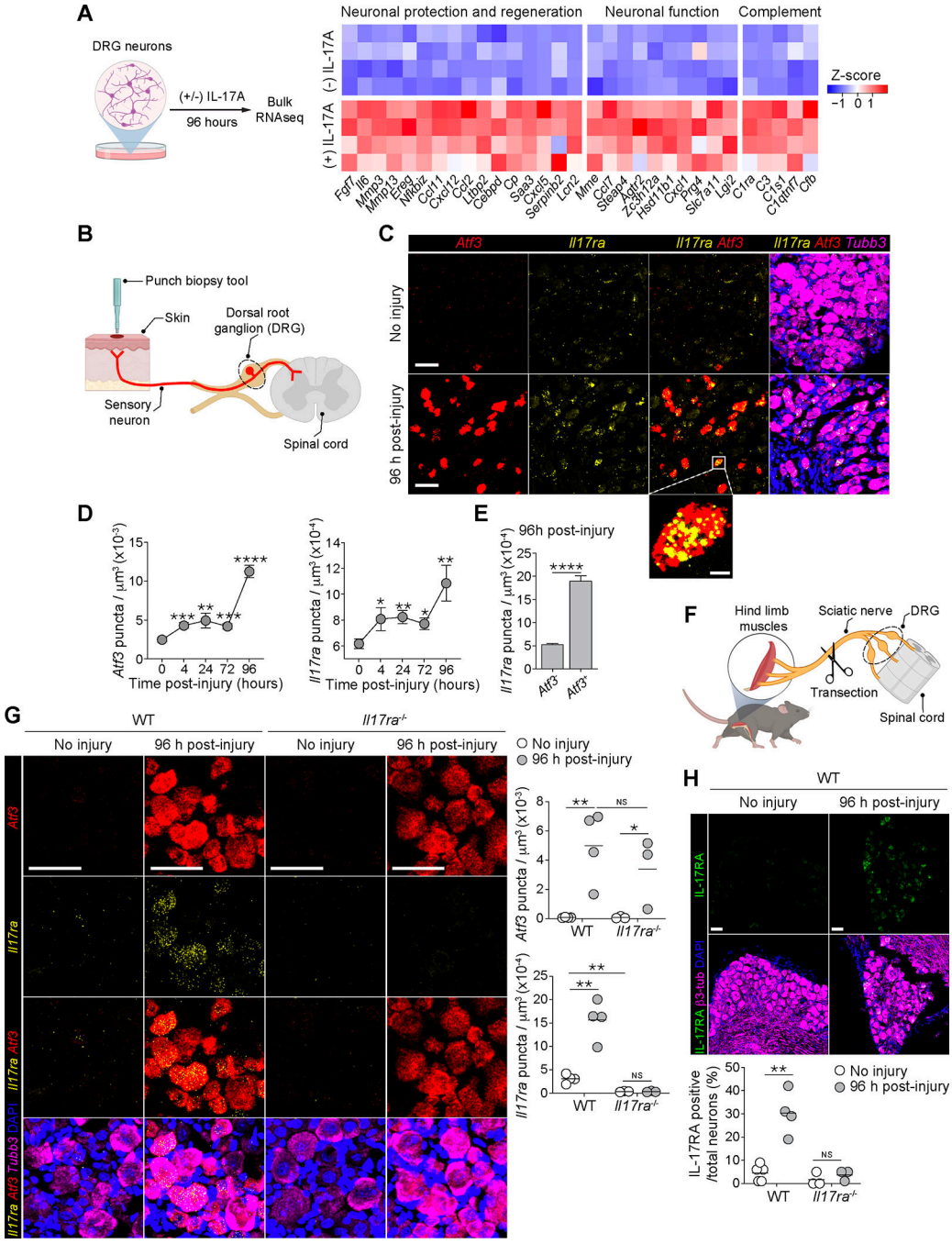

Figure 4. *Il17ra* is upregulated by injured neurons

(A) DRG neurons were cultured in presence of IL-17A for 96 hours and analyzed by bulk RNA-seq (left). Heatmap (right) showing relative expression of differentially expressed genes between cultured DRG neurons treated with or without IL-17A.

(B) Diagram of punch biopsy and skin nerve innervation. Injured skin sensory neurons whose cell bodies reside in the DRG connect the damaged skin with the spinal cord.

(C) RNAscope images of the cervical-DRG2, stained with probes against mRNA transcripts encoding *Il17ra* (yellow), *Atf3* (red), and *Tubb3* (magenta).

(D) Quantification (mean ± SEM) of *Atf3* (left) and *Il17ra* (right) mRNA expression in the cervical DRG2.
(E) Quantification (mean ± SEM) of *Il17ra* mRNA in $Atf3^{+}$ and $Atf3^{-}$ nerve fibers.
(F) Diagram of sciatic nerve transection model.
(G) RNAscope images of the lumbar-DRG4, stained with probes against mRNA transcripts encoding *Il17ra* (yellow), *Atf3* (red), and *Tubb3* (magenta) (left). Quantification of *Atf3* and *Il17ra* mRNA expression (right).
(H) Confocal microscopy images of the lumbar-DRG3, stained with anti-IL-17RA (green), anti-β3-tubulin (magenta) and DAPI for nuclei (blue) (top). Quantification of IL-17RA protein expression (bottom).
Graphs in D, E and G show gene expression (number of puncta / μm^3) within a segmented neuron. Each dot in G, H represents an individual mouse. Scale bars (50 μm), except for zoom in image (C), where scale bar (5 μm).*p < 0.05, **p < 0.01, ***p < 0.001, and ****p < 0.0001 and “NS”, not significant as calculated with Student’s t test. See also Figure S4.

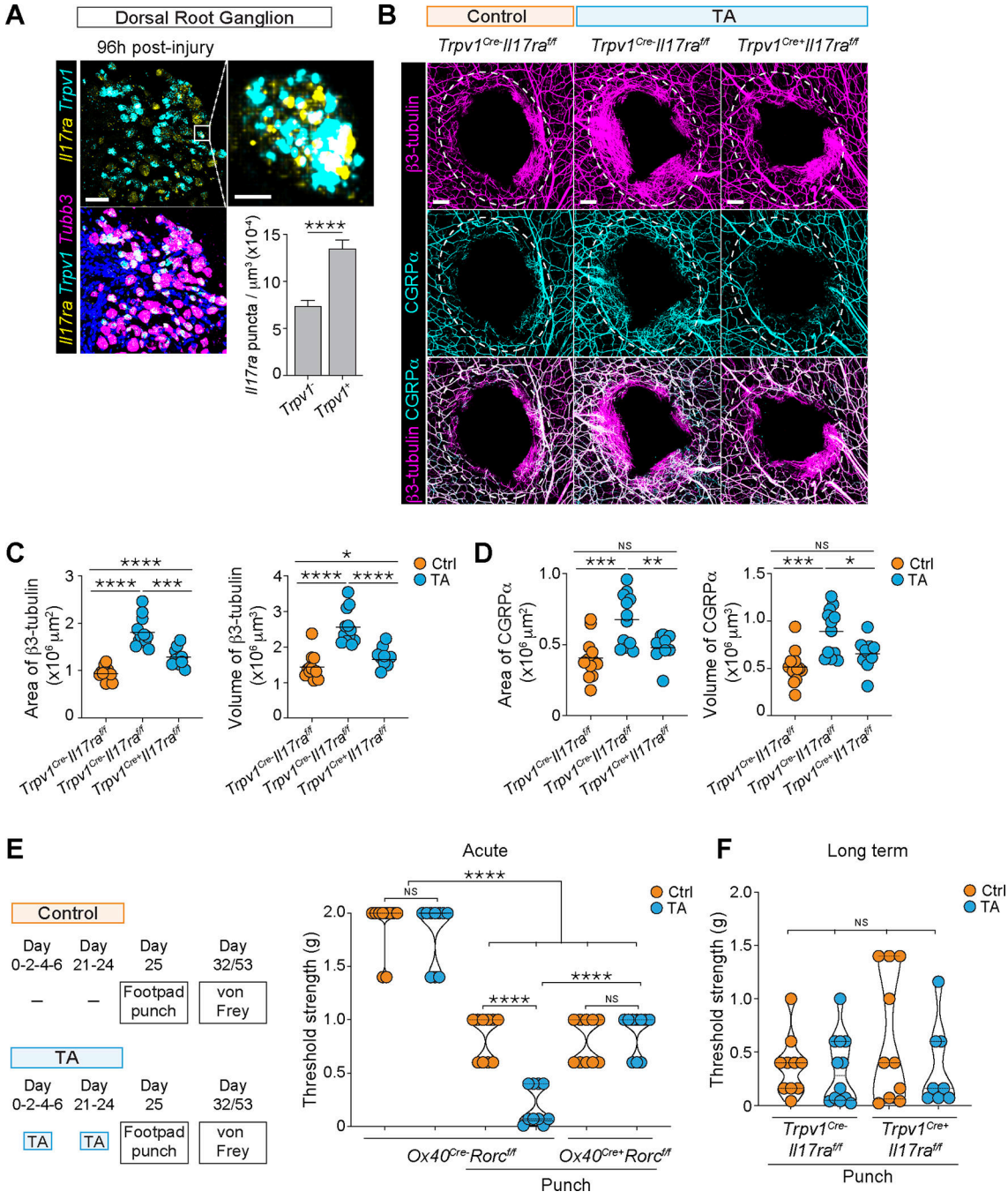

Figure 5. Neuronal IL-17RA signaling promotes sensory neuron regeneration and is not associated with aberrant mechanosensation.

(A) RNAscope images of the cervical-DRG2, stained with probes against mRNA transcripts encoding *Il17ra* (yellow), *Trpv1* (cyan), and *Tubb3* (magenta). Scale bar (50 µm), except for the zoom in image where the scale bar represents 5 µm. Quantification of *Il17ra* mRNA expression in *Trpv1*$^{+}$ and *Trpv1*$^{-}$ nerve fibers 96 hours post-injury. Bars are gene expression (number of puncta / µm^{3}) within a segmented neuron.

(B) Mice received two rounds of topical association (TA) with *S. aureus*. Subsequently the ear pinnae were injured by punch biopsy and analyzed by confocal microscopy 10 days later. Confocal images of the ring of nerve regeneration, stained with β3-tubulin and alpha-CGRP antibodies, in control (*Trpv1*$^{Cre-}$*Il17ra*$^{f/f}$) mice and mice lacking *Il17ra* expression in sensory neurons (*Trpv1*$^{Cre+}$*Il17ra*$^{f/f}$). Scale bars (200 μm).
(C) Area and volume quantification of the ring of neve regeneration (anti-β3-tubulin).
(D) Area and volume quantification of the ring of sensory neuron regeneration (anti-alpha-CGRP).
(E-F) Mice received two rounds of association (TA) with *S. aureus*. Subsequently, footpads were injured by punch biopsy and seven (E) or 28 (F) days later, mechanosensation was analyzed by von Frey test.
Data represent at least two experiments with three to four (A), 10 to 12 (C and D), and five to six (E and F) mice per group. Each dot represents an individual mouse (C and D) and the mechanical sensitivity threshold of an individual footpad (E and F). *$p < 0.05$, **$p < 0.01$, ***$p < 0.001$, and ****$p < 0.0001$ and “NS”, not significant as calculated with Student’s t test. See also Figure S5.

Key resources table

REAGENT or RESOURCE	SOURCE	IDENTIFIER
Antibodies		
Anti-mouse alpha-CGRP	Peninsula laboratories	Cat#T-4032; RRID: AB_518147
Anti-mouse CCR6, PE (29–2L17)	Biolegend	Cat#129804; RRID: AB_1279137
Anti-mouse CD3ε, PerCP-Cy5.5 (145–2C11)	eBioscience	Cat#45–0031–82; RRID: AB_1107000
Anti-mouse CD3ε, BV605 (145–2C11)	Biolegend	Cat#100351; RRID: AB_2565842
Anti-mouse CD4, AF700 (RM4–5)	eBioscience	Cat#56–0042–82; RRID: AB_494000
Anti-mouse CD4, BV605 (RM4–5)	Biolegend	Cat#100548; RRID: AB_2563054
Anti-mouse CD8α, PE (53–6.7)	eBioscience	Cat#12–0081–83; RRID: AB_465531
Anti-mouse CD8β, FITC (eBioH35–17.2)	eBioscience	Cat#11–0083–82; RRID: AB_657764
Anti-mouse CD8β, PE-Cy7 (eBioH35–17.2)	eBioscience	Cat#25–0083–82; RRID: AB_11218494
Anti-mouse CD8β, eFluor 450 (eBioH35–17.2)	eBioscience	Cat#48–0083–82; RRID: AB_11218504
Anti-mouse CD11b, PE-CF594 (M1/70)	BD Biosciences	Cat#562287; RRID: AB_11154216
Anti-mouse CD11b, eFluor 450 (M1/70)	eBioscience	Cat#48–0112–82; RRID: AB_1582236
Anti-mouse CD11b, BV605 (M1/70)	Biolegend	Cat#101257; RRID: AB_2565431
Anti-mouse CD11b, BV785 (M1/70)	Biolegend	Cat#101243; RRID: AB_2561373
Anti-mouse CD11c, APC-eFluor 780 (N418)	eBioscience	Cat#47–0114–82; RRID: AB_1548652
Anti-mouse CD11c, eFluor 450 (N418)	eBioscience	Cat#48–0114–82; RRID: AB_1548654
Anti-mouse CD11c, BV785 (N418)	Biolegend	Cat#117335; RRID: AB_11219204
Anti-mouse CD16/32 (2.4G2)	BioXCell	Cat#CUS-HB-197; RRID: AB_2687830
Anti-mouse CD19, PE/Dazzle 594 (6D5)	Biolegend	Cat#115553; RRID: AB_2564000
Anti-mouse CD19, eFluor 450 (1D3)	eBioscience	Cat#48–0193–82; RRID: AB_2043815
Anti-mouse CD24, FITC (M1/69)	Biolegend	Cat#101806; RRID: AB_312839
Anti-mouse CD31, AF647 (MEC13.3)	Biolegend	Cat#102516; RRID: AB_2161029
Anti-mouse CD44, PE-Cy7 (IM7)	eBioscience	Cat#25–0441–82; RRID: AB_469623
Anti-mouse CD44, AF700 (IM7)	eBioscience	Cat#56–0441–82; RRID: AB_494011
Anti-mouse CD45, APC-eFluor 780 (30-F11)	eBioscience	Cat#47–0451–82; RRID: AB_1548781
Anti-mouse CD45, BV510 (30-F11)	Biolegend	Cat#103138; RRID: AB_2563061
Anti-mouse CD45.1, FITC (A20)	eBioscience	Cat#11–0453–85; RRID: AB_465059
Anti-mouse CD45.1, BV510 (A20)	Biolegend	Cat#110741; RRID: AB_2563378
Anti-mouse CD45.2, APC-eFluor 780 (104)	eBioscience	Cat#47–0454–82; RRID: AB_1272175
Anti-mouse CD45.2, BV421 (104)	BD Biosciences	Cat#562895; RRID: AB_2737873
Anti-mouse CD49f, eFluor 450 (eBioGoH3)	eBioscience	Cat#48–0495–82; RRID: AB_11042564
Anti-mouse CD62L, FITC (MEL-14)	eBioscience	Cat#11–0621–85; RRID: AB_465110
Anti-mouse CD62L, AF700 (MEL-14)	eBioscience	Cat#56–0621–82; RRID: AB_2572047
Anti-mouse CD64, PerCP-Cy5.5 (X54–5/7.1)	Biolegend	Cat#139308; RRID: AB_2561963
Anti-mouse CD64, BV421 (X54–5/7.1)	Biolegend	Cat#139309; RRID: AB_2562694
Anti-mouse CD69, APC (H1.2F3)	Biolegend	Cat#104514; RRID: AB_492843
Anti-mouse CD90.2, BV605 (53–2.1)	Biolegend	Cat#140318; RRID: AB_2650924

REAGENT or RESOURCE	SOURCE	IDENTIFIER
Anti-mouse CD90.2, BV785 (30-H12)	Biolegend	Cat#105331; RRID: AB_2562900
Anti-mouse CD103, PerCP-eFluor 710 (2E7)	eBioscience	Cat#46–1031–82; RRID: AB_2573704
Anti-mouse/human Foxp3, FITC (FJK16s)	Invitrogen	Cat#11–5773–82
Anti-mouse Foxp3, AF700 (FJK-16s)	Invitrogen	Cat#56–5773–82
Anti-mouse Gata-3, eFluor 660 (TWJA)	eBioscience	Cat#50–9966–42
Anti-mouse GFRa-2	R and D Systems	Cat#AF429; RRID: AB_2294621
Anti-mouse IFN-γ, eFluor450 (XMG1.2)	eBioscience	Cat#48–7311–82; RRID: AB_1834366
Anti-mouse IFN-γ, AF488 (XMG1.2)	Invitrogen	Cat#53–7311–82
Anti-mouse IL-17A, PECy7 (TC11–18H10.1)	Biolegend	Cat#506922; RRID: AB_2125010
Anti-mouse IL-17RA	Abcam	Cat#ab180904; RRID: AB_2756838
Anti-mouse Ly-6C, BV605 (HK1.4)	Biolegend	Cat#128036; RRID: AB_2562353
Anti-mouse Ly-6G, PE-Cy7 (1A8)	BD Biosciences	Cat#560601; RRID: AB_1727562
Anti-mouse Ly-6G, BV421 (1A8)	Biolegend	Cat#127628; RRID: AB_2562567
Anti-mouse MHC-II, PE/Dazzle 594 (M5/114.15.2)	Biolegend	Cat#107648; RRID: AB_2565979
Anti-mouse MHC-II, eFluor 450 (M5/114.15.2)	eBioscience	Cat#48–5321–82; RRID: AB_1272204
Anti-mouse MHC-II, AF700 (M5/114.15.2)	eBioscience	Cat#56–5321–82
Anti-mouse NK1.1, eFluor 450 (PK136)	eBioscience	Cat#48–5941–82; RRID: AB_2043877
Anti-mouse RORγt, PE (B2D)	eBioscience	Cat# 12–6981–82; RRID: AB_10807092
Anti-human/mouse T-bet, BV421 (eBio4B10)	Biolegend	Cat#644816; RRID: AB_10959653
Anti-mouse TCRβ, PerCP-Cy5.5 (H57–597)	eBioscience	Cat#45–5961–82; RRID: AB_925763
Anti-mouse TCRγδ, eFluor 450 (eBioGL3)	eBioscience	Cat#48–5711–82; RRID: AB_2574071
Anti- mouse TCR Vγ1.1, APC (2.11)	Biolegend	Cat#141108; RRID: AB_10901177
Anti-mouse TCR Vγ3, FITC (536)	BD Biosciences	Cat#553229; RRID: AB_394721
Anti- mouse TCR Vγ3, APC (536)	Biolegend	RRID: AB_10895900 Cat# 137506
Anti-βIII Tubulin, NL557 (Tuj-1)	R & D Systems	Cat#NL1195R; RRID: AB_1241876
Anti-βIII Tubulin, APC (Tuj-1)	R & D Systems	Cat#IC1195A; RRID: AB_10571218
Anti-mouse Vβ14 FITC (14.2)	BD Biosciences	Cat#553258; RRID: AB_394738
Anti-mouse Vβ8.1.2 PE (MR5–2)	BD Biosciences	Cat#553186; RRID: AB_394695
Normal Goat Serum	Jackson ImmunoResearch Laboratories	Cat#005–000-121; RRID: AB_2336990
Rat Gamma Globulin	Jackson ImmunoResearch Laboratories	Cat#012–000–002; RRID: AB_2337135
Normal rabbit Serum	Jackson ImmunoResearch Laboratories	Cat#011–000–120; RRID: AB_2337123
Bacterial and virus strains		
Staphylococcus aureus 42F02	Laboratory of Dr. Julie Segre (NHGRI/NIH) Tamoutounour, S.[20]	N/A
Staphylococcus aureus HV1043	Laboratory of Dr. Julie Segre (NHGRI/NIH)	N/A
Staphylococcus aureus NCTC8325ΔtarS	Laboratory Michael Fischbach (Stanford University)	N/A
Staphylococcus aureus P6.34	Laboratory of Dr. Julie Segre (NHGRI/NIH)	N/A

REAGENT or RESOURCE	SOURCE	IDENTIFIER
Staphylococcus aureus NCTC8325	Laboratory of Dr. Julie Segre (NHGRI/NIH) Naik, S.[2]	N/A
Staphylococcus epidermidis NIHLM087	Laboratory of Dr. Julie Segre (NHGRI/NIH) Naik, S.[21]	N/A
Chemicals, peptides, and recombinant proteins		
2-Mercaptoethanol (1,000X)	Gibco	Cat#21985–023
2-Mercaptoethanol	Sigma-Aldrich	Cat#M3148–25ML
BSA	Sigma-Aldrich	Cat#A3059–500G
Brefeldin A (GolgiPlug)	BD Biosciences	Cat#555029
DAPI	Sigma-Aldrich	Cat#D9542
DMEM medium	Corning	Cat#10–017-CV
DNase I	Sigma-Aldrich	Cat#DN25–5G
EDTA (0.5M)	Corning	Cat#46–034-Cl
FBS	Hyclone	Cat#SH30070.03
L-Glutamine	Corning	Cat#25–005-Cl
HEPES	Corning	Cat#25–060-Cl
Ionomycin	Sigma-Aldrich	Cat#I0634–5MG
Liberase TL	Roche	Cat#05401020001
MEM Non-essential Amino Acids (100X)	Corning	Cat#25–025-Cl
Paraformaldehyde	Electron Microscopy Sciences	Cat#15714-S
Pennicillin-Streptomycin (100X)	Corning	Cat#30–002-Cl
Phorbol 12-myristate 13-acetate (PMA)	Sigma-Aldrich	Cat#P8139–10MG
ProLong Gold Antifade Mountant	Molecular Probes	Cat#P36930
RNAlater	Sigma-Aldrich	Cat#R0901–100ML
RPMI 1640 medium	Corning	Cat#10–040-CV
Sodium Pyruvate (100X)	Corning	Cat#25–000-Cl
Triton X	Sigma-Aldrich	Cat#T9284
Critical commercial assays		
RNAscope® Multiplex Fluorescent Reagent Kit v2	ACD	Cat#323100
BD Cytofix/Cytoperm	BD Biosciences	Cat#554722
BD Perm/Wash	BD Biosciences	Cat#554723
Foxp3 / Transcription Factor Staining Buffer Set	eBioscience	Cat#00–5523–00
High Sensitivity D1000 ScreenTape	Agilent	Cat#5067–5584
LIVE/DEAD Fixable Blue Dead Cell Staining Kit	Life Technologies	Cat#L23105
MACS Cell Separation Column LS	Miltenyi Biotec	Cat#130–042–401
NextSeq 500/550 v2 kits (75 cycles)	Illumina	Cat#FC-404–2005
Qubit dsDNA HS Assay Kit	Molecular Probes	Cat#Q32854
Deposited data		
Raw RNA-Seq data	This manuscript	NCBI, GSE196994
Experimental models: Organisms/strains		

REAGENT or RESOURCE	SOURCE	IDENTIFIER
Mouse: SA1 (S-*aureus*-specific TCR transgenic CD4 T cells mouse)	This manuscript	Mouse strain: SA1
Mouse: C57BL/6	Taconic	Mouse strain: B6
Mouse: CD45.1 (B6.SJL-Ptprc^{a} Pepc^{b}/BoyJ)	NIAID-Taconic Exchange	Mouse strain: Tac 8478
Mouse: C57BL/6-Tbet-ZsGreen[Tg] (T-bet-ZsGreen)	NIAID-Taconic Exchange	Mouse strain: Tac 8419
Mouse: CD45.1.2 (C57BL/6J × B6.SJL-CD45^{a}(Ly5^{a})/Nai F1)	NIAID-Taconic Exchange	Mouse strain: Tac 8422
Mouse: *Rag1*$^{-/-}$ (BG.SJ L-CD45^{a}Ly5^{a}Nai-[KO] RAG 1)	NIAID-Taconic Exchange	Mouse strain: Tac 165
Mouse: B6.129X1-*Gt(ROSA)*$^{26Sor\text{tm1(EYFP)Cos}}$/J (R26-stop-EYFP)	Jackson Laboratory	Mouse strain: Jax 006148
Mouse: *Il17a*$^{-/-}$ (C57BL/6-[KO]IL17A)	NIAID-Taconic Exchange	Mouse strain: Tac 8434
Mouse: Foxp3GFP reporter (C57BL/6-Foxp3^{tm1Kuch})	NIAID-Taconic Exchange	Mouse strain: Tac 382
Mouse: *Il1r1*$^{-/-}$ (C57BL/6-[KO]IL1r1)	NIAID-Taconic Exchange	Mouse strain: Tac 189
Mouse: IL-17A-Cre	Jackson Laboratory	Mouse strain: Jax 016879
Mouse: Albino B6 (C57BL/6NTac- *Tyr*^{tm1Arte})	NIAID-Taconic Exchange	Mouse strain: Jax 11971
Mouse: *Ox40*^{Cre} (B6.129X1(Cg)-*Tnfrsf4*$^{tm2(cre)Nik}$/J)	Laboratory of Remy Bosselut (NCI/NIH)	Mouse strain: Jax 012839
Mouse: *Rorc*$^{flox/flox}$ (B6(Cg)-*Rorc*$^{tm3Litt/J}$)	Jackson Laboratory	Mouse strain: Jax 008771
Mouse: *Trpv1*^{Cre} (B6.129-*Trpv1*$^{tm1(cre)Bbm}$/J)	Jackson Laboratory	Mouse strain: Jax 017769
Mouse: *Il17ra*$^{flox/flox}$ (B6.Cg-*Il17ra*$^{tm2.1Koll}$/J)	Jackson Laboratory	Mouse strain: Jax 031000
Mouse: *Atf3-IRES-Cre* mice	Laboratory of Claire Le Pichon (NIH). Nguyen, M.Q.[53]	N/A
Mouse : *Il17ra*$^{-/-}$	Amgen	N/A
Mouse: Alpha-CGRP-GFP (Calca$^{tm1.1(EGFP/HBEGF)Mjz}$)	Laboratory of John O'Shea (NIAID)	N/A
Mouse: ROSA-tdTomato (B6.Cg-*Gt(ROSA)26Sor*$^{tm14(CAG-tdTomato)Hze}$/J)	Jackson Laboratory	Mouse strain: Jax 007914
Mouse: *Lta*$^{-/-}$ (B6.129S2-Lta^{tm1Dch}/J)	Jackson Laboratory	Mouse strain: Jax 002258
Oligonucleotides		
RNAscope probe *Atf3* C1	ACD	Cat#426891
RNAscope probe *Atf3* C2	ACD	Cat#426891-C2
RNAscope probe *Atf3* C3	ACD	Cat#426891-C3
RNAscope probe *Trpv1* C3	ACD	Cat#313331-C3
RNAscope probe *Il17ra C2*	ACD	Cat#403741-C2
RNAscope probe custom *Il17ra-O C2*	ACD	Cat#1120081-C2
RNAscope probe *Tubb3* C1	ACD	Cat#423391
RNAscope probe *Tubb3* C2	ACD	Cat#423391-C2
RNAscope probe *Tubb3* C3	ACD	Cat#423391-C3
Software and algorithms		
Prism software	GraphPad	Version 9.3.1

REAGENT or RESOURCE	SOURCE	IDENTIFIER
Flowjo software	Becton Dickinson & Company (BD)	Version 10.6.1
Imaris software	Bitplane	Version 9.7.2
Other		
Opal 520	Akoya	Cat#FP1487001 KT
Opal 570	Akoya	Cat#FP1488001 KT
Opal 690	Akoya	Cat#FP1497001 KT